DESY 16-106, TTP16-023

$\overline{\rm MS}$-on-shell quark mass relation up to four loops in QCD and a general SU(N) gauge group

Peter Marquard[a], Alexander V. Smirnov[b],
Vladimir A. Smirnov[c], Matthias Steinhauser[d], David Wellmann[d]

(a) Deutsches Elektronen-Synchrotron, DESY 15738 Zeuthen, Germany

(b) Research Computing Center, Moscow State University
119991, Moscow, Russia

(c) Skobeltsyn Institute of Nuclear Physics of Moscow State University
119991, Moscow, Russia

(d) Institut für Theoretische Teilchenphysik, Karlsruhe Institute of Technology (KIT)
76128 Karlsruhe, Germany

Abstract

In this paper we compute the relation between heavy quark masses defined in the modified minimal subtraction and on-shell scheme. Detailed results are presented for all coefficients of the SU(N_c) colour factors. The reduction of the four-loop on-shell integrals is performed for a general QCD gauge parameter. Some of the about 380 master integrals are computed analytically, others with high numerical precision based on Mellin-Barnes representations, and the rest numerically with the help of `FIESTA`. We discuss in detail the precise numerical evaluation of the four-loop master integrals. Updated relations between various short-distance masses and the $\overline{\rm MS}$ quark mass to next-to-next-to-next-to-leading order accuracy are provided for the charm, bottom and top quark. We discuss the dependence on the renormalization and factorization scale.

PACS numbers: 12.38.Bx, 12.38.Cy, 14.65.Fy, 14.65.Ha

1 Introduction

Quark masses are fundamental parameters of Quantum Chromodynamics (QCD) and thus it is mandatory to determine their numerical values as precise as possible. Furthermore, it is important to have precise relations at hand which relate the masses in different renormalization schemes.

The renormalization scheme for the quark masses has to be fixed once quantum corrections are considered. In QCD there are two distinct renormalization schemes for the quark masses: the on-shell (OS) scheme, which is motivated by the physical interpretation of the mass parameter, and the modified minimal subtraction ($\overline{\mathrm{MS}}$) scheme which is very convenient for many practical calculations, in particular in high-energy reactions.

In the case of the lighter quarks (up, down and strange) the meson masses are in general much heavier than the masses of the quarks. Thus, the concept of the on-shell scheme is not applicable to light quark flavours; their numerical values are usually given in the $\overline{\mathrm{MS}}$ scheme. On the other hand, the mesons involving charm and bottom quarks are essentially dominated by the quark masses. For this reason, the quantum corrections considered in this paper are mainly relevant for the three heavy quarks, charm, bottom and top.

The top quark plays a special role in this context. Due to its large width it decays before hadronization and thus can be considered as an almost free quark. As a consequence it can be expected that the on-shell value for the top quark can be determined with a relative small uncertainty. This aspect has been studied in detail in the recent works [1,2]. It has been shown that the on-shell top quark can be computed from the $\overline{\mathrm{MS}}$ mass with an irreducible uncertainty of about 70 MeV [2].

There are various methods to determine the numerical values of the quark masses. Some of them determine directly the $\overline{\mathrm{MS}}$ quark mass (see, e.g., Ref. [3]) and thus do not suffer from the inherent renormalon ambiguity. However, the highest sensitivity to the quark masses is in general obtained from physical quantities evaluated at energies close to the quark mass, so-called threshold quantities. In such situations it is in general not possible to use the $\overline{\mathrm{MS}}$ scheme for the renormalization of the heavy quark. To nevertheless avoid the renormalon ambiguity the so-called threshold masses have been invented. Among the most prominent ones are the potential subtracted (PS) [4], 1S [5–7], renormalon subtracted (RS) [8] and the kinetic mass [9].[1] They allow for a precise determination of the heavy $\overline{\mathrm{MS}}$ mass without explicit reference to the pole. However, in intermediate steps the pole mass and in particular the relation between the pole and the $\overline{\mathrm{MS}}$ mass is still needed.

In the following we describe three typical examples where the four-loop term in the mass relations turns out to be important.

- At the TEVATRON and the LHC the top quark mass is measured with an uncer-

[1] Note that the relation of the kinetic mass to the on-shell mass is currently only known to NNLO. For this reason it will not be considered in the following.

tainty below 1 GeV. For example, the combination of results from ATLAS, CDF, CMS and D0 from March 2014 [10] leads to

$$M_t = 173.34 \pm 0.27(\mathrm{stat}) \pm 0.71(\mathrm{syst})\ \mathrm{GeV}\,, \tag{1}$$

with a total uncertainty of 760 MeV. The value in Eq. (1) is often called "Monte-Carlo mass" and there are several attempts which suggest methods to relate it to the on-shell mass (see, e.g., Refs. [11–13]). In case Eq. (1) is interpreted as the on-shell quark mass it has to be converted to the $\overline{\mathrm{MS}}$ top quark mass. Note that the three-loop term in the conversion formulae contributes approximately 500 MeV which is of the same order as the experimental uncertainties in Eq. (1).

- From measurements of the top quark pair production cross section close to threshold at a future linear collider it will be possible to determine the top quark threshold mass with an accuracy below 100 MeV (see, e.g., Refs. [14,15]). In the conversion to the $\overline{\mathrm{MS}}$ definition there is a contribution of about 150-200 MeV from the three-loop term in the mass relations which contributes significantly to the final uncertainty of the $\overline{\mathrm{MS}}$ mass (see Section 4.2 for precise numbers). With the help of the four-loop $\overline{\mathrm{MS}}$-on-shell relation this uncertainty can be drastically reduced.

- The bottom quark mass can be extracted from Υ sum rules (see Refs. [16,17] for recent N^{3}LO analyses) and from $M(\Upsilon(1S))$ [18–20]. Usually, in a first step a threshold mass is obtained. To be able to compare with the $\overline{\mathrm{MS}}$ quark mass (as, e.g., extracted from low-moment sum rules [3]) one has to apply the corresponding conversion formula. At three loops the contribution is of the order of 30 MeV, which is of the same order of magnitude (in some cases even larger) than the combination of all other involved uncertainties.

These examples show that the three-loop contribution is sizeable and thus a reliable estimate of the uncertainty is only obtained once the four-loop corrections are available. Furthermore, note that for the PS, 1S and RS masses one knows the relation to the pole mass to N^{3}LO. However, due to strong cancellations (see below) the N^{3}LO term cannot be used unless four-loop corrections to the $\overline{\mathrm{MS}}$ and on-shell quark mass are available.

The remainder of the paper is organized as follows: In the next Section we introduce the conversion factor between the on-shell and the $\overline{\mathrm{MS}}$ mass and discuss the colour decomposition of the four-loop term. Furthermore, we provide several technical details and discuss in particular the numerical accuracy of the master integrals. Section 3 is devoted to the results of the $\overline{\mathrm{MS}}$-on-shell relation which we discuss for the physical limit, i.e. $N_c = 3$ and fixed number of massless quarks, n_l, but also for generic N_c and even for general SU(N_c) colour factors. Several application of the $\overline{\mathrm{MS}}$-on-shell relation are discussed in Section 4 and our conclusions are contained in Section 5.

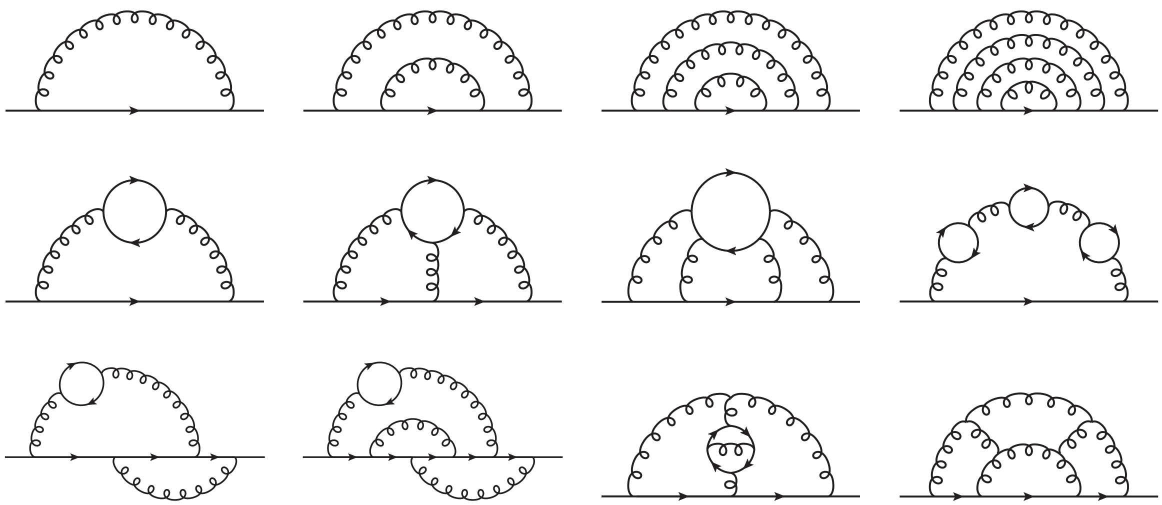

Figure 1: Sample Feynman diagrams contributing to Σ_S and Σ_V at one-, two-, three- and four-loop order. The solid lines represent quarks and the curly lines gluons.

2 Technicalities

2.1 Mass relations

The relation between the bare (m_0) and renormalized mass in the $\overline{\rm MS}$ scheme (m) is given by

$$m_0 = Z_m^{\overline{\rm MS}} m \,, \tag{2}$$

where $Z_m^{\overline{\rm MS}}$ only contains poles in ϵ. It is obtained by requiring that the renormalized propagator is finite. Note that in QCD the fermion propagator contains two Lorenz structures (scalar and vector) and thus next to $Z_m^{\overline{\rm MS}}$ also the $\overline{\rm MS}$ wave function renormalization constant is determined. $Z_m^{\overline{\rm MS}}$ has been computed to five-loop order in Ref. [21]; for our calculation only four-loop corrections [22–24] are needed, in particular the results for generic SU(N_c) colour factors which can be extracted from the anomalous dimension given in [23]. For convenience we present the result for $Z^{\overline{\rm MS}}$ in Appendix F. Note that the $\overline{\rm MS}$-renormalized mass m depends on the renormalization scale μ which is suppressed in Eq. (2). $Z_m^{\overline{\rm MS}}$ depends on μ via the strong coupling constant $\alpha_s(\mu)$.

In the on-shell renormalization scheme one requires that the quark two-point function has a zero at the position of the on-shell mass M which fixes the renormalization constant $Z_m^{\rm OS}$ introduced via

$$m_0 = Z_m^{\rm OS} M \,. \tag{3}$$

Note that m_0 and M are μ-independent and $Z_m^{\rm OS}$ contains $\alpha_s(\mu)$ and $\log(\mu/M)$ terms. The on-shell wave function renormalization constant is determined from the requirement that the quark propagator has a residuum $-i$ for $q^2 \to M^2$. This leads to a formula for $Z_2^{\rm OS}$ which is independent from $Z_m^{\rm OS}$. This is different in the $\overline{\rm MS}$ scheme where $Z_m^{\overline{\rm MS}}$ and $Z_2^{\overline{\rm MS}}$ have to be determined simultaneously.

A formula for $Z_m^{\rm OS}$ is conveniently derived by considering the renormalized quark propagator which is given by

$$S_F(q) \;=\; \frac{-iZ_2^{\rm OS}}{\not q\; - m_{q,0} + \Sigma(q,M)}\,, \tag{4}$$

$\Sigma(q,M)$ is the (amputated) quark self energy which can be split into a scalar and vector contribution

$$\Sigma(q,M) \;=\; M\,\Sigma_S(q^2,M) + \not q\;\Sigma_V(q^2,M)\,, \tag{5}$$

where Σ_S and Σ_V only depend of q^2, the (renormalized) quark mass and μ (which is again suppressed). They are obtained from the self energy Σ with the help of the projectors

$$\Sigma_S((M^2,M) \;=\; \frac{1}{4M}\,{\rm Tr}\,\left(\Sigma(q,M)\right)\Big|_{q^2=M^2}\,, \tag{6}$$

$$\Sigma_V((M^2,M) \;=\; \frac{1}{4q^2}\,{\rm Tr}\,\left(\not q\;\Sigma(q,M)\right)\Big|_{q^2=M^2}\,. \tag{7}$$

Requiring that the inverse quark propagator, $[S_F(q)]^{-1}$ has a zero at the position of the on-shell mass, i.e.

$$S_F(q) \;\stackrel{q^2\to M^2}{\longrightarrow}\; \frac{-i}{\not q\; - M}\,, \tag{8}$$

leads to

$$Z_m^{\rm OS} \;=\; 1 + \Sigma_S(M^2,M) + \Sigma_V(M^2,M)\,. \tag{9}$$

Thus, for the evaluation of the n-loop contribution to $Z_m^{\rm OS}$ n-loop integrals have to be computed where the external momentum is on-shell, i.e., we have $q^2 = M^2$.

In this paper we will present results for the the finite quantity

$$z_m(\mu) \;=\; \frac{m(\mu)}{M} \;=\; \frac{Z_m^{\rm OS}}{Z_m^{\overline{\rm MS}}}\,, \tag{10}$$

which is obtained from Eqs. (2) and (9). Note that $z_m(\mu)$ depends on $\alpha_s(\mu)$ and $\log(\mu/M)$ and has the following perturbative expansion

$$z_m(\mu) \;=\; \sum_{n\ge 0}\left(\frac{\alpha_s(\mu)}{\pi}\right)^n z_m^{(n)}(\mu)\,, \tag{11}$$

with $z_m^{(0)} = 1$. For later convenience we decompose $z_m^{(n)}(\mu)$ into

$$z_m^{(n)}(\mu) \;=\; z_m^{(n)}(M) + z_m^{(n),\log}\,, \tag{12}$$

where the second term on the right-hand side comprises the μ-dependent terms which vanish for $\mu = M$. Analytic results for $z_m^{(n),\log}$ are given in Appendix C.

For later use we also introduce the inverted relation to Eq. (10)

$$c_m(\mu) \;=\; \frac{M}{m(\mu)}\,, \tag{13}$$

with

$$c_m(\mu) \;=\; \sum_{n\geq 0}\left(\frac{\alpha_s(\mu)}{\pi}\right)^n c_m^{(n)}(\mu)\,, \tag{14}$$

and $c_m^{(0)} = 1$. $c_m^{(n)}(\mu)$ is a function of $\log(\mu/m(\mu))$. Furthermore, we assume the analog decomposition of Eq. (12) with $c_m^{(n),\log} = 0$ for $\mu = m(m)$.

In this paper we consider generic SU(N_c) colour factors and present results for the coefficients. The four-loop term of Eq. (11) can be decomposed into 23 colour structures which are given by

$$\begin{aligned} z_m^{(4)} \;=\;& C_F^4 z_m^{FFFF} + C_F^3 C_A z_m^{FFFA} + C_F^2 C_A^2 z_m^{FFAA} + C_F C_A^3 z_m^{FAAA} \\ &+ \frac{d_F^{abcd} d_A^{abcd}}{N_c} z_m^{d_{FA}} + n_l \frac{d_F^{abcd} d_F^{abcd}}{N_c} z_m^{d_{FF}L} + n_h \frac{d_F^{abcd} d_F^{abcd}}{N_c} z_m^{d_{FF}H} \\ &+ C_F^3 T n_l z_m^{FFFL} + C_F^2 C_A T n_l z_m^{FFAL} + C_F C_A^2 T n_l z_m^{FAAL} \\ &+ C_F^2 T^2 n_l^2 z_m^{FFLL} + C_F C_A T^2 n_l^2 z_m^{FALL} + C_F T^3 n_l^3 z_m^{FLLL} \\ &+ C_F^3 T n_h z_m^{FFFH} + C_F^2 C_A T n_h z_m^{FFAH} + C_F C_A^2 T n_h z_m^{FAAH} \\ &+ C_F^2 T^2 n_h^2 z_m^{FFHH} + C_F C_A T^2 n_h^2 z_m^{FAHH} + C_F T^3 n_h^3 z_m^{FHHH} \\ &+ C_F^2 T^2 n_l n_h z_m^{FFLH} + C_F C_A T^2 n_l n_h z_m^{FALH} + C_F T^3 n_l^2 n_h z_m^{FLLH} \\ &+ C_F T^3 n_l n_h^2 z_m^{FLHH}\,, \end{aligned} \tag{15}$$

where C_F and C_A are the eigenvalues of the quadratic Casimir operators of the fundamental and adjoint representation for the SU(N_c) colour group, respectively, $T = 1/2$ is the index of the fundamental representation, and n_l and n_h count the number of massless and massive (with mass M) quarks. In this paper we have $n_h = 1$. It is nevertheless convenient to introduce the variable n_h. d_F^{abcd} and d_A^{abcd} are the symmetrized traces of four generators in the fundamental and adjoint representation, respectively. The colour structures in Eq. (15) are related to N_c via

$$C_F = \frac{N_c^2 - 1}{2N_c}\,, \qquad C_A = N_c\,, \qquad T = \frac{1}{2}\,,$$

$$d_F^{abcd}d_F^{abcd} = \frac{(N_c^2-1)(N_c^4-6N_c^2+18)}{96N_c^2}\,,$$
$$d_F^{abcd}d_A^{abcd} = \frac{N_c(N_c^2-1)(N_c^2+6)}{48}\,. \tag{16}$$

In the case of QCD we have $N_c = 3$.

One-, two- and three-loop QCD results to $Z_m^{\rm OS}$ have been computed in Refs. [25], [26] and [27–30], respectively, and electroweak effects have been considered in Refs. [31–37]. In Ref. [38] the four-loop results for z_m have been presented for $N_c = 3$ and $n_l = 3, 4$ and 5 with a numerical precision of 3% in the four four-loop coefficient evaluated for $\mu = M$. It is the aim of the present paper to generalize the findings of [38] to general N_c and arbitrary n_l. Furthermore, the precision is significantly improved. In this paper we will not study light-quark mass effects which are known at two [26] and three loops [39].

The relations between the threshold and the $\overline{\rm MS}$ masses are too long so that we refrain from printing them in explicit form. For practical purposes it is convenient to use their implementation in `RunDec` [40] and `CRunDec` [41]. The construction of the relations can be found in the original literature [4–8], a summary can, e.g., be found in Ref. [38].

2.2 Reduction to master integrals

For the calculation of Σ_S and Σ_V we use a highly automated and well-established set-up based on `qgraf` [42], `q2e` and `exp` [43, 44] and in-house `Mathematica` and `FORM` [45, 46] programs which work hand-in-hand to minimize the manual interaction. Colour factors are computed with the help of `color` [47].

For the generation of the amplitudes for the fermion propagator we use `qgraf` which generates 3100 diagrams. They are converted to `FORM` code using `q2e` and `exp`. A further task of the program `exp` is to map each diagram to one out of a set of 102 predefined integral families which are shown in graphical form in Appendix A. To obtain these families we start with the 11 prototypes shown in Fig. 2. They serve as basis to generate the allowed families by considering all possible routings of a massive line through the diagrams. Diagrams with self-energy insertions can be obtained by removing some lines and raising the propagator powers of other lines. For convenience we show a graphical representation for each family in Appendix A. At four loops, they are labeled by 14 indices which are powers of propagators and irreducible numerators. The maximal number of positive indices is eleven.

We use in-house `FORM` programs to apply the projectors to the vector and scalar part of the fermion propagator needed for the on-shell quark mass, perform traces and do the numerator algebra. As an outcome our result is written as a linear combination of scalar Feynman integrals which are related by integration-by-parts identities [48]. We apply to each family the Laporta algorithm [49] as implemented in `FIRE` [50–52] and `Crusher` [53] to perform a reduction to master integrals.

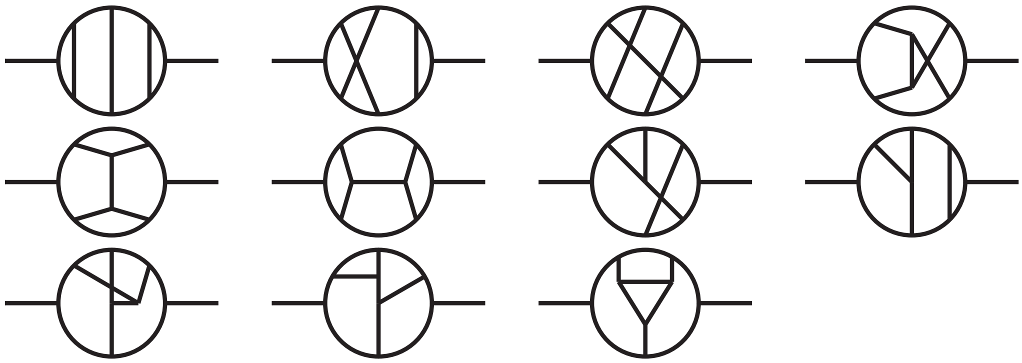

Figure 2: Four-loop prototype families needed to generate the four-loop on-shell integral families shown in Appendix A.

We first work with each of the individual families and reveal the corresponding master integrals. It turns out that the primary sets of the master integrals revealed with `FIRE` are not minimal, i.e. there exist additional relations among them. Then, following recipes of [51], we find additional relations using symmetries of various integrals with indices $0, 1$, and 2. For each sector (i.e. a subset of indices where some indices are positive and the other indices are non-positive), one can estimate the number of the master integrals using the code `Mint` [54]. There are, however, extra relations which connect master integrals of partially overlapping sectors and they can be revealed by the same procedure based on symmetries. The numbers of the master integrals in our families are big, up to 176.

One more criterion when looking for additional relations is the absence of spurious dependence of denominators in reduction relations on d. The general analysis of singularities of Feynman integrals as functions of d shows that poles in d can be only real rational numbers. So, if we observe a non-factorizable polynomial of second or higher degree in d in a denominator this means that either we miss a relation between current master integrals or some master integrals are chosen in an inappropriate way. At least in all the cases in our calculation, we managed to get rid of such spurious denominators by revealing additional relations or making better choices of the master integrals. However, with the sets of master integrals we have arrived at it is not guaranteed that we have really minimal sets of master integrals, i.e. bases of the corresponding linear spaces.

The next step was to find relations between master integrals of various families. To do this, we use the Mathematica code `tsort` which is part of the latest `FIRE` version [52] and end up with 386 four-loop massive on-shell propagator integrals, i.e. with $q^2 = M^2$.

We have performed the calculation allowing for a general gauge parameter ξ keeping terms up to order ξ^2 in the expression we give to the reduction routines. We have checked that ξ drops out after adding counterterm contributions from mass renormalization which is a welcome cross check on the consistency of our result.

As was mentioned above the algorithms we use to minimize the number of basis integrals does not guarantee that we obtain all relations among the integrals which appear as masters of the individual families. The fact that ξ drops out before using explicit results for the master integrals is a hint that we are at least close to the minimal set.

We refrain from listing all master integrals but provide some examples in the next subsection where the numerical accuracy of those integrals is discussed which cannot be computed analytically.

Let us stress that up to this point our calculation is completely analytical.

2.3 Computation of master integrals

In this subsection we want to describe our methods which we used to obtain results for the master integrals.

All master integrals are computed numerically with the help of `FIESTA` [55–57]. `FIESTA` applies the sector decomposition algorithm which leads to a, in general, multi-dimensional integral representation of the coefficients of the ϵ expansion. The integration is performed using Monte-Carlo methods as implemented in the `CUBA` [58] library. `FIESTA` allows for a highly parallel numerical integration and provides an almost linear scaling behaviour. In fact, most of our calculations are performed at the High Performance Computing Center Stuttgart (HLRS) and the Supercomputing Center of Lomonosov Moscow State University which provide up to 1024 CPU cores or 64 Tesla GPUs for a single run. The integral data base obtained with `FIESTA` provides the reference for the improvements for some of the integrals discussed in the following.

We have computed all integrals using different statistics ranging from $N = 0.5 \times 10^6$ to $N = 2 \times 10^6$ sampling points. We have observed that the uncertainty decreases proportional to $1/\sqrt{N}$ according to the expectations for Monte-Carlo integrations. In Fig. 3 we show three typical master integrals which are shown in graphical form to the left of the plot. For each term of the ϵ expansion, which are indicated on the x axis, several data points are shown which correspond to different number of sampling points.[2] The central values are normalized to the most precise result and then we subtract 1 which explains why the central value of the leftmost data point is equal to 0. The uncertainty bars correspond to the results where the Monte-Carlo uncertainty based on `Vegas` [59] is multiplied by a factor ten (see also discussion below).

For the first two examples we observe that the central values of the more precise calculation lies within the uncertainties of the less precise ones. At the same time the uncertainty is significantly reduced.[3] The third example behaves differently: For the ϵ^1 and ϵ^2 terms we observe a relatively big jumps after increasing the sampling points from $N = 5 \times 10^7$ to $N = 5 \times 10^8$ and then to $N = 2 \times 10^9$. Furthermore, the more precise central value lies

[2]For better readability the results for different sampling points are slightly displaced.

[3]In those cases where the uncertainty does not become smaller after increasing the sampling points the requested precision is already reached for a smaller number of sampling points.

partly outside the ten-sigma uncertainty bands.

We have produced the convergence plots as those in Fig. 3 for all master integrals computed with `FIESTA`. Note that the one in the bottom panel of Fig. 3 is among the integrals with the worst behaviour. Altogether for about five master integrals the five-sigma uncertainty band is not sufficient to find agreement between the central values of the high-precision results with the uncertainty band of the low-precision results. For this reason we adopt a conservative attitude and multiply the Monte-Carlo uncertainty of `FIESTA` by a factor ten. The reason for such a multiplication can also be justified by the fact that each master integral leads to thousands individual sector integrals, and each of them produces some error estimate. `FIESTA` uses the mean-square norm when adding up error estimates, but in unlucky situations this might be not enough for a real error estimate.

It turns out that some of the master integrals revealed with `FIRE`, which have usually indices equal to 1 and 0, are not optimal for the subsequent numerical evaluation with `FIESTA`, i.e. the achieved precision of the numerical evaluation is not the best one. In such situations, we tried to make a better choice of the master integrals replacing master integrals of some sector by other integrals which can have indices equal to 2. In some cases, we successfully followed the strategy advocated in Ref. [60] where the goal was to choose a finite or a quasi-finite (in the sense that the only divergence comes from the overall gamma function in Feynman parametrization) basis.

In particular, for our final result we replaced the integral shown on the bottom panel of Fig. 3 by an integral with numerators which shows a much better convergence behaviour. Let us, however, stress that the final results (discussed in the next Section) for the two different basis are consistent within the uncertainties.

For all factorizable integrals, we obtained analytic results from known one-, two- and three-loop results. In particular, we use the results of Ref. [61] where all three-loop master integrals have been obtained in an ϵ expansion up to the order typical to four-loop calculations. For four of them, G43, G53, G62, and G65 (see Fig. 3 of [61]) we had to add one more order in ϵ which is straightforward. In most cases one can derive a one-dimensional Mellin-Barnes representation which converges exponentially and thus $\mathcal{O}(1000)$ digits can easily be obtained. In our calculation we encounter in total seven factorizable integrals.

For some master integrals, analytic results could be derived using a straightforward loop-by-loop integration at general d, see, e.g., Fig. 5 (top, leftmost). We also used analytical results obtained for the 13 non-trivial four-loop on-shell master integrals computed in our earlier paper [62] (see Figs. 3 and 4 of [62]).

At this point we take over a practical attitude and generate an ordered list which contains the ϵ coefficients of master integrals with large contributions to the final uncertainty. This list is used as a basis to improve step-by-step the accuracy of our result by increasing the numerical precision of the corresponding master integral. Up to a certain point this could be reached by simply increasing the statistics in the approach based on `FIESTA`. Of course,

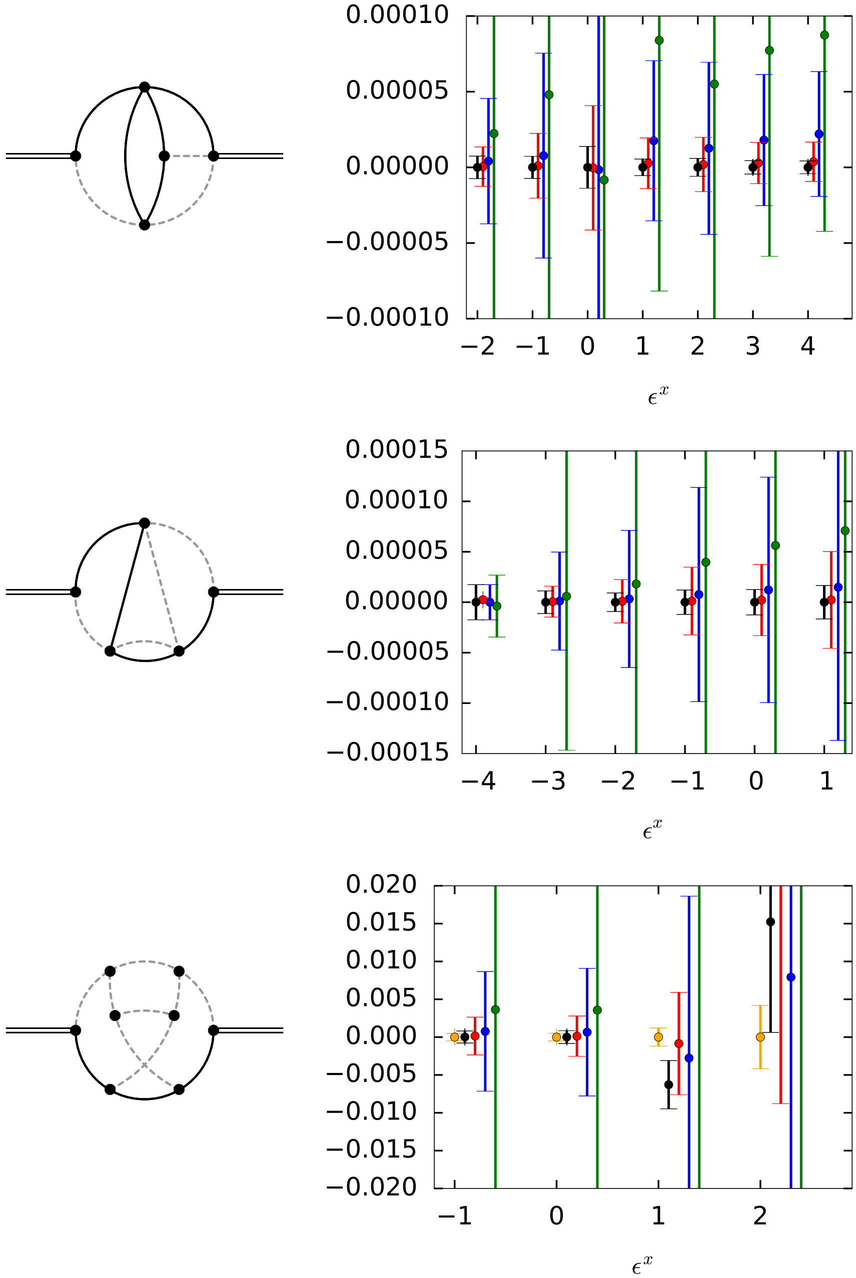

Figure 3: `FIESTA` results for three typical integrals for various choices of N. The corresponding master integrals are shown to the left of the plots (see caption of Fig. 4 for the meaning of the lines). In this plot the `FIESTA` uncertainties have been multiplied by a factor ten. For each ϵ coefficient on the x axis results for different number of sampling points, N, are shown. For all plots we show results for $N = 5 \times 10^k$ with $k = 5, 6, 7, 8$. The bottom plot also contains results for $N = 2 \times 10^9$. In each case we normalize the results to the most precise one and then subtract 1.

this approach is quite limited since an increase of the number of sample points by ten leads to an uncertainty which is reduced by about a factor three.

A closer look to the generated list shows that the major contribution to the uncertainty comes from master integrals containing two- or three-point sub-diagrams. For these integrals we proceed as follows:

- *Derive Mellin-Barnes representations for the subdiagrams.*
  This is achieved with the help of the formula

$$\frac{1}{(X+Y)^{\lambda}} = \frac{1}{\Gamma(\lambda)}\frac{1}{2\pi i}\int_{-i\infty}^{+i\infty} \mathrm{d}z\, \frac{Y^{z}}{X^{\lambda+z}}\Gamma(\lambda+z)\Gamma(-z)\,, \tag{17}$$

  which is used to split sums in the denominator raised to arbitrary power into products. In this way massive propagators can be transformed into massless ones at the cost of a Mellin-Barnes integration. It is worth to mention, that it does not need any specific hierarchy among the summands. Depending on the other lines of the original diagram we use the Mellin-Barnes method such that the external momenta of the subdiagram are either massive or massless. If possible, we apply on-shell conditions for external momenta.

  As an example we present our results for two typical "building blocks".

  – The bubble integral with two massive lines (see Fig. 4, second diagram of first row) with massless external legs can be written in the following form

$$\begin{aligned}
&\int \frac{\mathrm{d}^d k}{i\pi^{\frac{d}{2}}} \frac{1}{[m^2-k^2]^{a_1}[m^2-(k+p)^2]^{a_2}} = \\
&\quad \frac{1}{2\pi i}\int_{-i\infty}^{+i\infty} \mathrm{d}z\, \frac{(m^2)^{\frac{d}{2}-a_1-a_2-z}}{(-p^2)^{-z}} \\
&\quad \times \frac{\Gamma(-z)\Gamma(a_1+z)\Gamma(a_2+z)\Gamma(a_1+a_2-\frac{d}{2}+z)}{\Gamma(a_1)\Gamma(a_2)\Gamma(a_1+a_2+2z)}\,.
\end{aligned} \tag{18}$$

  – The triangle integral with two massive internal lines as well as one massive, one massless and one leg that is on-shell (see Fig. 4, first diagram of second row) is given by

$$\begin{aligned}
&\int \frac{\mathrm{d}^d k}{i\pi^{\frac{d}{2}}} \frac{1}{[m^2-(k+p_1)^2]^{a_1}[m^2-(k+p_1+p_2)^2]^{a_2}[-k^2]^{a_3}} = \\
&\quad \frac{1}{(2\pi i)^2}\int_{-i\infty}^{+i\infty} \mathrm{d}z_1 \mathrm{d}z_2\, \frac{(m^2)^{\frac{d}{2}-a_1-a_2-a_3-z_1-z_2}}{(m^2-p_1^2)^{-z_1}(-p_2^2)^{-z_2}} \\
&\quad \times \frac{\Gamma(-z_1)\Gamma(-z_2)\Gamma(a_2+z_2)\Gamma(a_3+z_1)\Gamma(a_1+z_1+z_2)}{\Gamma(a_1)\Gamma(a_2)\Gamma(a_3)\Gamma(d-a_1-a_2-a_3)} \\
&\quad \times \frac{\Gamma(d-a_1-a_2-2a_3-z_1)\Gamma(a_1+a_2+a_3-\frac{d}{2}+z_1+z_2)}{\Gamma(a_1+a_2+z_1+2z_2)}\,.
\end{aligned} \tag{19}$$

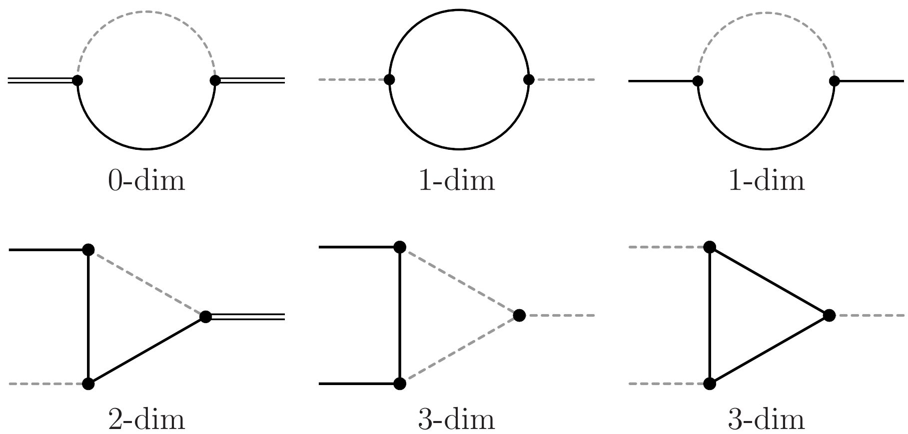

Figure 4: Sample building blocks for the loop-by-loop approach with three different types of external legs: dashed or solid lines denote massless- or massive propagators of general momentum p^2 respectively. Their general complex powers can depend on the dimensional regularization parameter ϵ and Mellin-Barnes integration variable z_i. Double lines are on-shell with the condition $p^2 = m^2$. The dimension of the Mellin-Barnes integration is specified below the diagrams.

Note that the exponents in Eqs. (18) and (19) need not to be integer but may also depend on ϵ.

- *Decompose integral into products of building blocks.*
  The derived building blocks are applied step-by-step until all momentum integrations are replaced by Mellin-Barnes integrals. For simple integrals one ends up with a two- or three-dimensional integration (cf. Fig. 5). In theses cases a precision of about nine digits is achieved for the ϵ^6 terms. The coefficients of the lower ϵ orders are more precise. We also encountered higher-dimensional integrals which lead to a lower precision. Some examples with five, six or even seven dimensional integrations can be found in Fig. 5. For these case one obtains about five digits for the ϵ^0 and two to three digits for the ϵ^3 term.

  It is interesting to note that the decomposition into building blocks is not unique. In fact, different representations may have significantly different convergence properties which we exploited for some of the integrals.

Altogether we have treated 80 master integrals with the help of the described method. The results of the Mellin-Barnes integrals are usually quite precise for lower orders of the ϵ expansion and give several digits more than `FIESTA` provides. For 16 out of 80 integrals FIESTA produced better results in the higher-orders of ϵ and we choose to compose "hybrid" results where the lower orders were taken from the MB-integrals and the ϵ^3 or higher terms came from `FIESTA`.

For the preparation of the Mellin-Barnes integrals we use the package `MB` [63] together with its extensions discussed in Ref. [64]. For the numerical integration we use the integrator

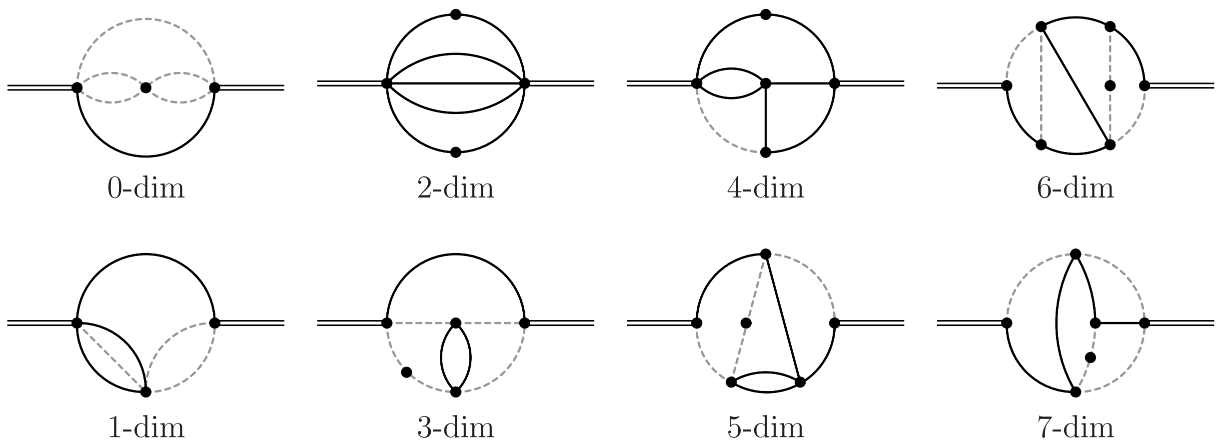

Figure 5: Sample master integrals which are treated with the Mellin-Barnes method. The dimension of the Mellin-Barnes integration is specified below the diagrams.

`cuhre` as implemented in the `CUBA` library [58]. As far as our experience goes the estimated uncertainty of `cuhre` is too small which can be seen by comparing the results of the numerical integration to (analytically) known results. Thus, we multiply the uncertainty by a factor 100 to be on the conservative side. For the higher-dimensional integrals we have also tried to use `vegas`, however, could not increase the precision [65].

We have compared all 80 master integrals computed with the Mellin-Barnes method with the `FIESTA` results and found good agreement for almost all ϵ coefficients within three standard deviations. However, in a few cases deviations up to seven sigma are observed which once again justifies to use a conservative limit of ten sigma for the Monte-Carlo uncertainty of `FIESTA` [65].

The systematic application of the Mellin-Barnes method is the main source for the improvements as compared to the results presented in Ref. [38].

The described procedure can, of course, only be applied to a subset of all master integrals. However, as mentioned above, in our basis these kinds of integrals provide the substantial part to the uncertainty to z_m in case we use the results based on `FIESTA`.

For the remaining 259 integrals (i.e. the ones which are neither known analytically nor treated with the Mellin-Barnes method) we use the `FIESTA` result. When inserting the master integrals we keep track of all uncertainties and combine them quadratically in the final expression. We interpret the resulting uncertainty as a standard deviation and multiply it by ten (as justified above) in the final result for the relation between the $\overline{\text{MS}}$ and on-shell quark mass. Note, in case we add the uncertainties from the individual contributions linearly we obtain an uncertainty which is about five times larger than the uncertainty resulting from the quadratic combination. For example, $z_m^{(4)}$ for $N_c = 3$ and $n_l = 5$ reads -871.732 ± 0.180 for quadratic and -871.732 ± 0.872 for linear combination (without security factor 10).

3 Results for the $\overline{\text{MS}}$-on-shell relation

As an outcome of the procedure discussed in the previous Section we obtain bare four-loop results for $\Sigma_V(q^2 = M_q^2) + \Sigma_S(q^2 = M_q^2)$ which still contain forth-order poles in the regularization parameter ϵ. Furthermore, uncertainties from each ϵ order of the numerically evaluated master integrals are present in the expression. The individual uncertainties shall eventually be combined quadratically to obtain the final uncertainty. It is obvious that the latter is sensitive to whether

- $N_c = 3$ (and optionally also a value for n_l) is chosen before combining the uncertainties from the master integrals,
- the expression is parameterized in terms of generic N_c and n_l,
- or even as a linear combination of the SU(N_c) Casimir invariants.

In this Section we will discuss all three options. Note that we interpret the final uncertainty as a standard deviation which we multiply by a factor ten to be on the conservative side.

It is convenient to present results for the finite relation between the $\overline{\text{MS}}$ and on-shell mass. It is obtained after renormalization of the quark mass in the on-shell and the strong coupling constant in the $\overline{\text{MS}}$ scheme using three-loop renormalization constants. Whereas α_s is renormalized by a simple multiplicative factor it is convenient to generate the mass counterterm contribution simultaneously to the lower-order contributions. A finite quantity is obtained after dividing the (parameter renormalized) Z_m^{OS} by $Z_m^{\overline{\text{MS}}}$, as discussed around Eq. (10).

To obtain an impression about the quality of the cancellations of the poles we present in the following table results for three typical contributions to $z_m^{(4)}$ $(\mu^2 = M^2)$

	$z_m^{(4)}$ for $N_c = 3$, $n_l = 5$			coef. of N_c^4 term			coef. of C_F^4 term		
ϵ^{-4}	-0.00001	$\pm$	0.00002	-0.0000002	$\pm$	0.0000002	-0.000006	$\pm$	0.000013
ϵ^{-3}	0.0003	$\pm$	0.0002	0.000002	$\pm$	0.000002	0.0001	$\pm$	0.0001
ϵ^{-2}	-0.0002	$\pm$	0.0018	0.000001	$\pm$	0.000016	-0.0007	$\pm$	0.0009
ϵ^{-1}	0.0044	$\pm$	0.0191	0.00002	$\pm$	0.00018	0.0005	$\pm$	0.0081
ϵ^{0}	-871.732	$\pm$	0.180	-51.181	$\pm$	0.002	-6.983	$\pm$	0.081

Note that the uncertainties are the ones returned from the numerical integration without introducing any security factor. Still, all pole coefficients are zero within one standard deviation which shows that the factor ten applied to the final results presented below is conservative.

From now on we only consider ϵ^0 terms. Furthermore, we choose $\mu^2 = M^2$ (for z_m) or $\mu^2 = m^2(\mu^2)$ (for c_m). The renormalization scale dependent terms can be computed

n_l	$z_m^{(4)}(M)$			$c_m^{(4)}(m)$		
0	−3654.15	±	1.64	3567.60	±	1.64
1	−2940.01	±	1.67	2864.60	±	1.67
2	−2308.77	±	1.70	2244.32	±	1.70
3	−1756.36	±	1.74	1702.70	±	1.74
4	−1278.70	±	1.77	1235.66	±	1.77
5	−871.73	±	1.80	839.14	±	1.80
6	−531.39	±	1.84	509.07	±	1.84
7	−253.59	±	1.87	241.37	±	1.87
8	−34.28	±	1.91	31.99	±	1.91
9	130.62	±	1.94	−123.15	±	1.94
10	245.17	±	1.98	−228.12	±	1.98
11	313.45	±	2.01	−286.98	±	2.01
12	339.51	±	2.05	−303.81	±	2.05
13	327.44	±	2.08	−282.68	±	2.08
14	281.30	±	2.12	−227.64	±	2.12
15	205.16	±	2.16	−142.78	±	2.16
16	103.09	±	2.19	−32.15	±	2.19
17	−20.85	±	2.23	100.16	±	2.23
18	−162.58	±	2.26	250.10	±	2.26
19	−318.03	±	2.30	413.59	±	2.30
20	−483.15	±	2.34	586.56	±	2.34

Table 1: Results for $z_m^{(4)}(M)$ and $c_m^{(4)}(m)$ for $N_c = 3$ and $0 \leq n_l \leq 20$.

analytically using renormalization group techniques; they are given in Appendix C.

3.1 Results for $N_c = 3$

We start with specifying both N_c and n_l before combining the uncertainties from the master integrals. The results for $z_m^{(4)}(M)$ and $c_m^{(4)}(m)$ for $N_c = 3$ are shown in Table 1. Note that for the physical interesting cases $n_l = 4, 5$ and 6 we have a find a relative uncertainty between 0.1% and 0.2%.

From Table 1 one observes that the uncertainty has only a very mild dependence on n_l. Thus, to a good approximation we can write $z_m^{(4)}$ in the form[4]

$$z_m^{(4)} = -3654.15 \pm 1.64 + (756.942 \pm 0.040) n_l - 43.4824 n_l^2 + 0.678141 n_l^3 \,. \quad (20)$$

In Fig. 3.1 we plot Eq. (20) for n_l between 0 and 20 and combine the data points for integer n_l to guide the eye. It is interesting to note that the four-loop coefficient $z_m^{(4)}$

[4]Note, that this is not a fit to Table 1.

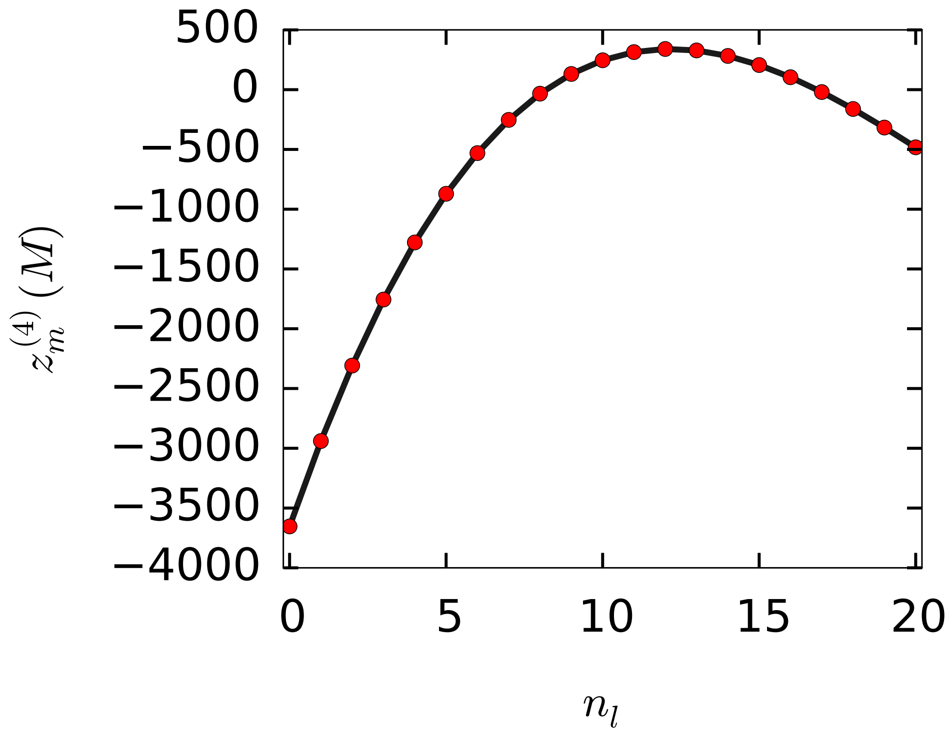

Figure 6: n_l-dependence of $z_m^{(4)}(M)$.

becomes positive between $n_l = 9$ and $n_l = 16$. Close to these value of n_l (i.e. for $n_l = 8$ and $n_l = 17$) the absolute value of $z_m^{(4)}$ is quite small and thus the relative uncertainty exceeds 5%.

The four-loop coefficient of the inverted relation, $c_m^{(4)}$, which is basically obtained from negative $z_m^{(4)}$ plus some products of lower order contributions, shows a similar behaviour except for the overall sign. It has, in particular, the same uncertainty, as can be seen in the last column of Table 1. The explicit n_l dependence reads

$$c_m^{(4)} \quad = \quad 3567.60 \pm 1.64 - (745.721 \pm 0.040) n_l + 43.3963 n_l^2 - 0.678141 n_l^3 \,. \qquad (21)$$

For some applications it is useful to have control over all fermionic contributions, including the ones from closed fermion loops of mass M which we label by n_h. The corresponding result is shown in Table 2 where we present the coefficients of $n_l^i n_h^j$ for $i, j = 0, 1, 2, 3$ with $i + j \leq 3$.

$n_l^0 n_h^0$	-3678.28	$\pm$	1.63
$n_l^0 n_h^1$	23.63	$\pm$	0.12
$n_l^0 n_h^2$	0.5273	$\pm$	0.0027
$n_l^0 n_h^3$	-0.02484	$\pm$	0.00000
$n_l^1 n_h^0$	757.64	$\pm$	0.04
$n_l^1 n_h^1$	-0.6646	$\pm$	0.0004
$n_l^1 n_h^2$	-0.03617	$\pm$	0.00000
$n_l^2 n_h^0$	-43.47	$\pm$	0.00
$n_l^2 n_h^1$	-0.01720	$\pm$	0.00000
$n_l^3 n_h^0$	0.6781	$\pm$	0.0000

Table 2: $z_m^{(4)}$ decomposed into coefficients of $n_l^i n_h^j$.

3.2 Results for generic N_c

In a next step we do not specify numerical values for N_c and n_l which leads to 23 non-zero colour structures. For the corresponding coefficients we obtain

$$
\begin{aligned}
z_m^{LLL1/N_c^1} &= -0.25430\,,\\
z_m^{LLLN_c^1} &= 0.25430\,,\\
z_m^{LL1/N_c^2} &= -0.14090\,,\\
z_m^{LL1/N_c^1} &= 0.00645\,,\\
z_m^{LLN_c^0} &= 5.58971\,,\\
z_m^{LLN_c^1} &= -0.00645\,,\\
z_m^{LLN_c^2} &= -5.44881\,,\\
z_m^{L1/N_c^3} &= 0.1788 \pm 0.0333\,,\\
z_m^{L1/N_c^2} &= -0.18076 \pm 0.00000\,,\\
z_m^{L1/N_c^1} &= 0.9282 \pm 0.0445\,,\\
z_m^{LN_c^0} &= 0.28392 \pm 0.00005\,,\\
z_m^{LN_c^1} &= -32.7991 \pm 0.0109\,,\\
z_m^{LN_c^2} &= -0.10316 \pm 0.00005\,,\\
z_m^{LN_c^3} &= 31.69215 \pm 0.00124\,,\\
z_m^{1/N_c^4} &= -0.4364 \pm 0.0503\,,\\
z_m^{1/N_c^3} &= 0.821 \pm 0.121\,,\\
z_m^{1/N_c^2} &= 0.1739 \pm 0.0738\,,\\
z_m^{1/N_c^1} &= 0.645 \pm 0.161\,,\\
z_m^{N_c^0} &= -0.614 \pm 0.175\,,\\
z_m^{N_c^1} &= -2.6228 \pm 0.0415\,,
\end{aligned}
$$

$$
\begin{aligned}
z_m^{N_c^2} &= 52.0579 \pm 0.0808\,, \\
z_m^{N_c^3} &= 1.15654 \pm 0.00424\,, \\
z_m^{N_c^4} &= -51.1812 \pm 0.0161\,,
\end{aligned}
\tag{22}
$$

where the notation used for the superscripts is self-explanatory.[5] The n_l^3 and n_l^2 terms are known analytically and can be found in Ref. [62, 66] (see Appendix E). Both for the linear-n_l and the n_l-independent contribution one obtains small (relative) uncertainties for the positive powers in N_c which dominate in the physical limit $N_c = 3$. This explains the small uncertainties of coefficients in the previous subsection.

From Eq. (22) one learns that the dominant uncertainty for the $N_c = 3$-result origins from the $z_m^{N_c^2}$, followed by the N_c-independent term $z_m^{N_c^0}$.

As a cross check we choose $N_c = 3$, fix n_l and use the coefficients of Eqs. (22) to compute $z_m^{(4)}$ combing all uncertainties again quadratically. We obtain the following results

n_l	$z_m^{(4)}$
3	-1756.36 ± 1.52
4	-1278.70 ± 1.53
5	-871.73 ± 1.53

The central values are by construction identical to the corresponding entries in Table 1, the uncertainties are even slightly smaller. This might happen since the uncertainties are added linearly when setting N_c and n_l to numerical values before combining the uncertainties from the individual ϵ terms (cf. Subsection 3.1). As compared to adding the uncertainties in quadrature this might lead to larger (as in the case at hand) or smaller (see next subsection) uncertainties.

3.3 Results in term of Casimir colour factors

This subsection is devoted to the most general results, namely z_m in the form of Eq. (15). For the coefficients of the 23 colour structures we obtain

$$
\begin{aligned}
z_m^{FFFF} &= -6.983 \pm 0.805\,, \\
z_m^{FFFA} &= 13.40 \pm 2.07\,, \\
z_m^{FFAA} &= -11.17 \pm 1.74\,, \\
z_m^{FAAA} &= -99.272 \pm 0.493\,, \\
z_m^{d_{FA}} &= 0.39 \pm 1.07\,, \\
z_m^{d_{FF}L} &= -0.937 \pm 0.178\,, \\
z_m^{d_{FF}H} &= -3.924 \pm 0.642\,,
\end{aligned}
$$

[5]Example: z_m^{L1/N_c^2} is the coefficient of n_l/N_c^2; "L" counts the factors n_l.

$$
\begin{aligned}
z_m^{FFFL} &= -0.05094 \pm 0.00298\,, \\
z_m^{FFAL} &= 9.26642 \pm 0.00454\,, \\
z_m^{FAAL} &= 122.1872 \pm 0.0100\,, \\
z_m^{FFLL} &= -2.25441\,, \\
z_m^{FALL} &= -42.46326\,, \\
z_m^{FLLL} &= 4.06885\,, \\
z_m^{FFFH} &= -1.3625 \pm 0.0132\,, \\
z_m^{FFAH} &= 14.9800 \pm 0.0334\,, \\
z_m^{FAAH} &= -2.3597 \pm 0.0342\,, \\
z_m^{FFHH} &= 1.65752 \pm 0.00031\,, \\
z_m^{FAHH} &= -0.20934 \pm 0.00273\,, \\
z_m^{FHHH} &= -0.14902 \pm 0.00000\,, \\
z_m^{FFLH} &= -2.89209 \pm 0.00010\,, \\
z_m^{FALH} &= 0.62076 \pm 0.00042\,, \\
z_m^{FLLH} &= -0.10321\,, \\
z_m^{FLHH} &= -0.21703 \pm 0.00000\,.
\end{aligned}
\tag{23}
$$

The n_l^3 and n_l^2 terms are known analytically and can be found in Appendix E. The linear-n_l term is dominated by z_m^{FAAL} which has an uncertainty below 0.01%. On the other hand, for z_m^{FFFL} the precision in only about 4%, however, the numerical impact is small, even for $N_c = 2$.

The contributions involving closed heavy quark loops are generally small and know to a precision of about 10% or better, the numerically dominant z_m^{FFAH} contribution even to about 1.3%.

There are five non-fermionic contributions, z_m^{FFFF}, z_m^{FFFA}, z_m^{FFAA}, z_m^{FAAA} and $z_m^{d_{FA}}$. The most precise one, z_m^{FAAA}, has the by far largest coefficient and furthermore the largest colour factor. The three coefficients z_m^{FFFF}, z_m^{FFFA} and z_m^{FFAA} have an uncertainty between 11% and 15%. $z_m^{d_{FA}}$ is the worst known coefficient. Actually, within our precision we cannot claim whether it is positive or negative. Note, however, that not only the coefficient itself but also the colour factor is numerically small as compared to others. For example, for $N_c = 3$ we have $d_F^{abcd} d_A^{abcd}/N_c = 15/6 = 2.5$ whereas $C_F C_A^3 = 36$. The current uncertainty of $z_m^{d_{FA}}$ is dominated by master integrals where we rely on the `FIESTA` results.

As a cross check we insert the results from Eq. (23) into Eq. (15) and specify the colour factors to their numerical values with $N_c = 3$. We add all uncertainties in quadrature and obtain

n_l	$z_m^{(4)}$
3	-1756.36 ± 36.3
4	-1278.70 ± 36.3
5	-871.73 ± 36.3

which has to be compared with the corresponding entries in Table 1 where $N_c = 3$ is chosen before combining the uncertainties from the individual master integrals. As expected, one observes the same central value, however, the uncertainties are significantly larger.

4 Applications

4.1 $\overline{\text{MS}}$-on-shell transformation formulae

In the following we discuss the relation between the $\overline{\text{MS}}$ and on-shell quark mass and specify the number of massless quarks to the top, bottom and charm case.

Let us start with the version where the on-shell mass is computed from the $\overline{\text{MS}}$ mass. We use as input the following $\overline{\text{MS}}$ masses

$$\begin{aligned} m_t(m_t) &= 163.508 \text{ GeV}\,, \\ m_b(m_b) &= 4.163 \text{ GeV}\,, \\ m_c(3 \text{ GeV}) &= 0.986 \text{ GeV}\,, \end{aligned} \tag{24}$$

where $m_t(m_t)$ is computed from $M_t = 173.34$ GeV [10] using four-loop accuracy. The $\overline{\text{MS}}$ masses for charm and bottom are taken from Ref. [3].

The values for the strong coupling are given by $\alpha_s^{(6)}(m_t) = 0.1085$, $\alpha_s^{(5)}(m_b) = 0.2253$, and $\alpha_s^{(4)}(3 \text{ GeV}) = 0.2540$. They have been computed from $\alpha_s^{(5)}(M_Z) = 0.1181$ using `RunDec` [40, 41]. In the case of the charm quark we also provide results for $\mu = m_c(m_c)$ using the input values $m_c(m_c) = 1.279$ GeV and $\alpha_s^{(4)}(m_c) = 0.3872$. Note that the choice $\mu = 3$ GeV is preferable since it has the advantage that low renormalization scales $\mu \approx m_c$ are avoided.

In the following equations we list the results for the relations which convert the $\overline{\text{MS}}$ to the on-shell mass. For simplicity we set here and in the remainder of this section the uncertainty of the four-loop coefficient to 0.2% although it is for charm and bottom slightly smaller (see Table 1).

$$\begin{aligned} M_t &= m_t(m_t)\left(1 + 0.4244\,\alpha_s + 0.8345\,\alpha_s^2 + 2.375\,\alpha_s^3 + (8.615 \pm 0.017)\,\alpha_s^4\right) \\ &= 163.508 + 7.529 + 1.606 + 0.496 + (0.195 \pm 0.0004) \text{ GeV}\,, \qquad (25) \\ M_b &= m_b(m_b)\left(1 + 0.4244\,\alpha_s + 0.9401\,\alpha_s^2 + 3.045\,\alpha_s^3 + (12.685 \pm 0.025)\,\alpha_s^4\right) \\ &= 4.163 + 0.398 + 0.199 + 0.145 + (0.136 \pm 0.0003) \text{ GeV}\,, \qquad (26) \\ M_c &= m_c(3 \text{ GeV})\left(1 + 1.133\,\alpha_s + 3.119\,\alpha_s^2 + 10.981\,\alpha_s^3 + (51.419 \pm 0.102)\,\alpha_s^4\right) \\ &= 0.986 + 0.284 + 0.198 + 0.177 + (0.211 \pm 0.0004) \text{ GeV}\,, \qquad (27) \\ M_c &= m_c(m_c)\left(1 + 0.4244\,\alpha_s + 1.0456\,\alpha_s^2 + 3.757\,\alpha_s^3 + (17.480 \pm 0.035)\,\alpha_s^4\right) \\ &= 1.279 + 0.210 + 0.200 + 0.279 + (0.503 \pm 0.001) \text{ GeV}\,, \qquad (28) \end{aligned}$$

where the renormalization scale of α_s in each equation is identical to the one specified for the $\overline{\mathrm{MS}}$ quark mass in the prefactor of the first lines in each equation.

One observes a good convergence for the top where the coefficients steadily decrease; the four-loop coefficient is more then a factor two smaller than the three-loop one. This is different for charm and bottom where the two-, three and four-loop coefficients are of the same order of magnitude. In Eq. (28) (where $\mu^2 = m_c^2$ has been chosen) the four-loop coefficient is even almost twice a large as the three-loop coefficient.

For convenience we also present the inverted relation of Eq. (25) which is given by

$$\begin{aligned} m_t(m_t) &= M_t \left(1 - 0.4244\,\alpha_s - 0.9246\,\alpha_s^2 - 2.593\,\alpha_s^3 - (8.949 \pm 0.018)\,\alpha_s^4\right) \\ &= 173.34 - 7.924 - 1.859 - 0.562 - (0.209 \pm 0.0004)\text{ GeV}\,, \end{aligned} \tag{29}$$

where $\alpha_s \equiv \alpha_s(M_t) = 0.1077$. We refrain from providing the analog equations for charm and bottom since this would require to specify the pole masses which we refrain from doing.

4.2 Relation between $\overline{\mathrm{MS}}$ and threshold mass

The threshold masses are constructed such that the relation to the $\overline{\mathrm{MS}}$ mass is well behaved in perturbation theory. It is illustrating to examine the cancellations which take place between the coefficients in the $\overline{\mathrm{MS}}$-OS relation and the ones in the relation of the OS and threshold mass. For example, in the case for the bottom quark mass we have for the PS mass

$$\begin{aligned} m_b^{\mathrm{PS}}(\mu_f = 2\text{ GeV}) &= 4.163 + (0.399 - 0.191) + (0.199 - 0.120) \\ &\quad +(0.145 - 0.114) + (0.1364 - 0.1368 \pm 0.0003)\text{ GeV} \\ &= 4.163 + 0.207 + 0.080 + 0.032 - (0.0004 \pm 0.0003)\text{ GeV}\,, \end{aligned} \tag{30}$$

where the second terms inside the round brackets after the first equality sign originate from the PS-OS relation. As expected due to the very definition of the PS mass, one observes a significant cancellation between the coefficients of the PS-OS and PS-$\overline{\mathrm{MS}}$ relation. The cancellation becomes stronger at higher loop-order. In particular, at four loops one observes a cancellation of three significant digits, which is the reason why four digits after the comma are provided. Note that the details of the cancellations depend on μ_f, as we will discuss in Section 4.3.

After the second equality sign the number in the round brackets are added. One observes a nice convergence behaviour with decreasing coefficients which has to be compared to the OS-$\overline{\mathrm{MS}}$ relation where the three- and four-loop coefficients have the same order of magnitude, cf. Eq. (26). The four-loop coefficient in Eq. (30) only amounts to -0.4 MeV which is actually of the same order of magnitude as the uncertainty. Note, however, that both the central value and the uncertainty are far below the expected precision of the $\overline{\mathrm{MS}}$ bottom quark mass within the foreseeable future.

The analog equation to (30) for the top quark reads

$$
\begin{aligned}
m_t^{\mathrm{PS}}(\mu_f = 80 \text{ GeV}) &= 163.508 + (7.531 - 3.685) + (1.607 - 0.989) \\
&\quad + (0.495 - 0.403) + (0.195 - 0.211 \pm 0.0004) \text{ GeV} \\
&= 163.508 + 3.847 + 0.618 + 0.092 - (0.016 \pm 0.0004) \text{ GeV} \,. \quad (31)
\end{aligned}
$$

Also here one observes a drastic reduction of the correction terms when going to higher orders. In fact, the last term amounts to only 16 MeV instead of 200 MeV in Eq. (25).

For the 1S mass we obtain the following perturbative relations to the $\overline{\mathrm{MS}}$ bottom and top mass

$$
\begin{aligned}
m_b^{1\mathrm{S}} &= 4.163 + (0.399 - 0.047) + (0.195 - 0.072) \\
&\quad + (0.139 - 0.100) + (0.129 - 0.137 \pm 0.0003) \text{ GeV} \\
&= 4.163 + 0.352 + 0.123 + 0.039 - (0.008 \pm 0.0003) \text{ GeV} \,, \\
m_t^{1\mathrm{S}} &= 163.508 + (7.531 - 0.428) + (1.588 - 0.368) \\
&\quad + (0.479 - 0.262) + (0.185 - 0.174 \pm 0.0004) \text{ GeV} \\
&= 163.508 + 7.103 + 1.220 + 0.217 + (0.011 \pm 0.0004) \text{ GeV} \,. \qquad (32)
\end{aligned}
$$

where the first and second number in the bracket origins from the OS-$\overline{\mathrm{MS}}$ and OS-1S relation, respectively. Furthermore, we order the terms according the ε expansion as defined in Refs. [5–7]. It is interesting to note that at LO (first round bracket) the contribution from the OS-1S relation amounts only to few per cent of the OS-$\overline{\mathrm{MS}}$ relation. At N^{3}LO, however, it is more than 90% both for bottom and top.

Similar results to those presented in Eqs. (30), (31) and (32) for bottom and top are also obtained for the charm quark in case $\mu = 3$ GeV is chosen for the renormalization scale. On the other hand, in case the relation of the threshold mass to $m_c(m_c)$ is computed the four-loop term exceeds the three-loop one. We furthermore observe that the relations to the RS and RS′ masses behave very similar to the PS and 1S masses. We refrain to provide explicit results which are easily obtained with the help of `RunDec` [40] and `CRunDec` [41].

In practice a threshold quark mass is extracted from comparison of experimental measurements and theory predictions. Afterwards it is converted to the $\overline{\mathrm{MS}}$ quark mass. In Table 3 we show the results for the scale invariant $\overline{\mathrm{MS}}$ quark masses $m_q(m_q)$ $(q = t, b, c)$ and $m_c(3 \text{ GeV})$ using one- to four-loop accuracy for the conversion. The input values for the threshold masses (which are provided at the top of each table) are chosen such that the four-loop results agree with the input values discussed in Eq. (24). For top a rapid convergence is observed with four-loop contributions between 10 and 20 MeV. The situation is similar for the bottom quark where the four-loop term amounts to at most 8 MeV for the case of the 1S mass. As already mentioned above, the four-loop term for the case where $m_c(m_c)$ is computed from the threshold masses is larger than the three-loop contribution which is different for $m_c(3 \text{ GeV})$ where the four-loop term is smaller by up to a factor four. Thus, even in this case we observe a reasonable convergence of

input	$m^{\mathrm{PS}} =$	$m^{1\mathrm{S}} =$	$m^{\mathrm{RS}} =$	$m^{\mathrm{RS}'} =$
#loops	168.049	172.060	166.290	171.785
1	164.174	164.904	163.702	164.226
2	163.580	163.727	163.520	163.591
3	163.492	163.519	163.490	163.500
4	163.508	163.508	163.508	163.508
4 (×1.002)	163.507	163.507	163.507	163.507

(a) $m_t(m_t)$

input	$m^{\mathrm{PS}} =$	$m^{1\mathrm{S}} =$	$m^{\mathrm{RS}} =$	$m^{\mathrm{RS}'} =$
#loops	4.481	4.668	4.364	4.692
1	4.266	4.308	4.210	4.286
2	4.191	4.192	4.173	4.196
3	4.163	4.155	4.159	4.165
4	4.163	4.163	4.163	4.163
4 (×1.002)	4.163	4.163	4.163	4.163

(b) $m_b(m_b)$

input	$m^{\mathrm{PS}} =$	$m^{1\mathrm{S}} =$	$m^{\mathrm{RS}} =$	$m^{\mathrm{RS}'} =$
#loops	1.130	1.513	1.035	1.351
1	1.255	1.342	1.249	1.146
2	1.230	1.250	1.273	1.276
3	1.235	1.214	1.249	1.250
4	1.279	1.279	1.279	1.279
4 (×1.002)	1.278	1.278	1.278	1.278

(c) $m_c(m_c)$

input	$m^{\mathrm{PS}} =$	$m^{1\mathrm{S}} =$	$m^{\mathrm{RS}} =$	$m^{\mathrm{RS}'} =$
#loops	1.153	1.545	1.043	1.357
1	1.077	1.261	1.028	1.074
2	1.021	1.117	1.008	1.020
3	0.993	1.032	0.992	0.995
4	0.986	0.986	0.986	0.986
4 (×1.002)	0.986	0.986	0.986	0.986

(d) $m_c(3\text{ GeV})$

Table 3: $m_q(m_q)$ ($q = t, b, c$) in GeV [see (a), (b), (c)] and $m_c(3\text{ GeV})$ (d) computed from the PS, 1S, RS and RS′ quark mass using LO to N^{3}LO accuracy. The numbers in the last line are obtained by taking into account the uncertainty of the four-loop coefficient, i.e., it is increased by 0.2%. This leads to a shift of at most 1 MeV. The factorization scales for the PS, RS and RS′ masses are set to 2 GeV for bottom and charm. For the top quark we use $\mu_f = 80$ GeV for the PS, RS and RS′ masses.

the perturbative series; for the PS and RS masses the N^{3}LO corrections are even below 10 MeV.

The results in Table 3 show that perturbatively well-behaved quark mass relations are obtained after introducing threshold masses. To exploit them at third order in perturbation theory, which is mandatory due to current precision reached for the quark masses, it is necessary to use four-loop relation between the on-shell and $\overline{\mathrm{MS}}$ quark mass for the construction of the $\overline{\mathrm{MS}}$-threshold mass relation.

To obtain the results in Table 3 we have set the renormalization scale in the relation between the threshold and $\overline{\mathrm{MS}}$ mass to the quark mass itself or to 3 GeV. As an alternative one could also apply the conversion relation at some intermediate scale μ and then run with four-loop accuracy in the $\overline{\mathrm{MS}}$ scheme for either the scale invariant mass or to $\mu = 3$ GeV for the charm quark. The corresponding results are shown in Fig. 7 where $m_t(m_t)$, $m_b(m_b)$ and $m_c(3\text{ GeV})$ are shown as a function of the intermediate scale μ. The panels on the left show the results for the PS mass for the one- to four-loop analysis. In all three cases one observes a rapid convergence when including higher order corrections resulting in an almost horizontal, i.e, μ independent, result at four loops.

The panels on the right compare the various threshold masses at three and four loops. Note that by construction the four-loop curves coincide for $\mu = m_q(m_q)$ for top and bottom and for $\mu = 3$ GeV for charm. In all cases one observes that the four loop curves are significantly flatter than the three-loop results. Particularly good results are obtained

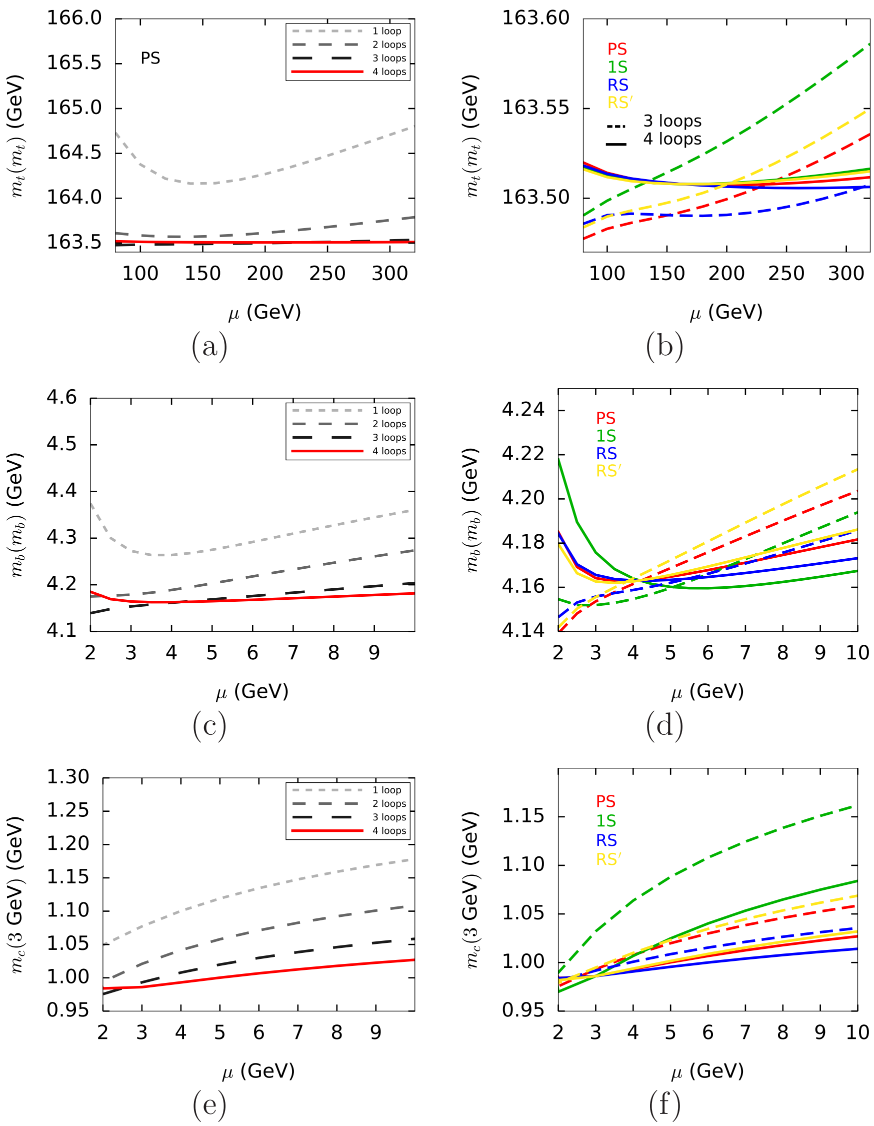

Figure 7: (a) $\overline{\text{MS}}$ top quark mass $m_t(m_t)$ computed from the PS mass with LO, NLO, NNLO and N^{3}LO accuracy as a function of the renormalization scale used in the $\overline{\text{MS}}$-threshold mass relation. (b) $\overline{\text{MS}}$ top quark mass $m_t(m_t)$ computed from the PS, 1S, RS and RS′ mass with NNLO (dashed) and N^{3}LO (solid line) accuracy as a function of the renormalization scale used in the $\overline{\text{MS}}$-threshold mass relation. At the right end of the plot the lines from bottom to top correspond to the RS, PS, RS′ 1S mass. (c)-(f) show the results for bottom and charm. For the bottom quark the four-loop result for the 1S mass is below (above) the others for high (low) values of μ.

for the top quark in panel (b) where in a large range the four-loop results lie on top of each other. The four-loop curves in the case of the bottom quark show stronger variations below, say, $\mu = 2.5$ GeV. Here the PS, RS and RS′ results are quite close together whereas the 1S curve shows a quite strong raise for $\mu \to 2$ GeV. Note that the scale on the y axis

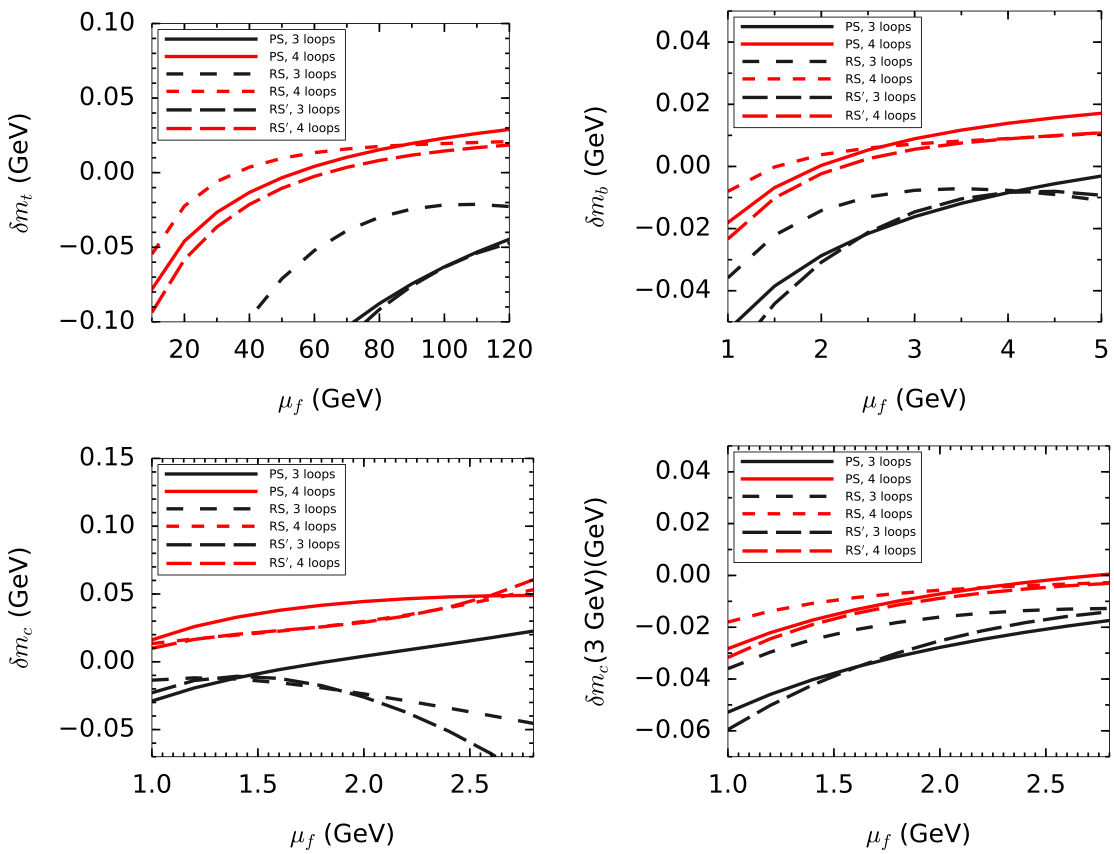

Figure 8: Three- (black, lower three curves in each plot) and four-loop (red, upper three curves in each plot) contribution in transition form PS, RS and RS′ mass to $m_q(m_q)$ and $m_c(3\text{ GeV})$ as a function of the factorization scale μ_f.

for the charm plot covers a bigger range than for the bottom bottom quark. Nevertheless the four-loop curve shows a quite flat behaviour. One observes again that the 1S curve deviates from the remaining ones.

4.3 μ_f dependence of PS, RS and RS′ mass

In this Section we study the dependence of the PS, RS and RS′ mass on the factorization scale μ_f. To do this we use $m_t(m_t)$, $m_b(m_b)$, $m_c(m_c)$ and $m_c(3\text{ GeV})$ from Eq. (24) and compute the threshold masses for the given value of μ_f to four-loop accuracy. This value is then used as starting point for the computation of the $\overline{\text{MS}}$ mass at one- to four-loop order as a function of μ_f. In Fig. 8 the three- (black) and four-loop (red) contributions to the conversion formula are plotted for the PS (solid) , RS (short dashes) and RS′ (long dashes) masses. In the case of the top quark the default scale for the PS mass suggested in Ref. [4] is $\mu_f = 20$ GeV. For this value the four-loop contribution amounts to about -50 MeV. One observes that the perturbative conversion formula is better behaved for larger values of μ_f. In fact, the four-loop term vanishes for $\mu_f \approx 50$ MeV and amounts to about $+10$ MeV for $\mu_f \approx 80$ MeV, a value suggested in Ref. [14] in the context of top quark pair production close to threshold. Similar conclusion also hold for the the RS and RS$'$ masses.

For the bottom quark the principle behaviour of the three- and four-loop correction terms is similar to the top quark case. Here, the suggested default value of $\mu_f = 2$ GeV [4, 8] seems to be a good choice from the perturbative point of view.

For completeness we show in Fig. 8 the corresponding results for the charm quark masses $m_c(m_c)$ and $m_c(3\text{ GeV})$. Here, the results are less conclusive, in particular for $m_c(m_c)$. Over a large range of μ_f the four-loop term is even larger than the three-loop contribution which is a sign that the formalism should not be applied to $m_c(m_c)$. The situation is better in case $m_c(3\text{ GeV})$ is considered, which is probably due to the smaller values of α_s (which increases significantly when going from $\mu = 3$ GeV to $\mu = m_c(m_c) \approx 1.3$ GeV). For $m_c(3\text{ GeV})$ the four-loop contribution is always smaller than the three-loop term, however, it comes close to zero only close to $\mu_f \approx 3$ GeV.

4.4 c_m in terms of $\alpha_s^{(n_l)}$

For certain applications (see, e.g, Ref. [2]) it is necessary to express the $\overline{\text{MS}}$-on-shell relation in terms of $\alpha_s^{(n_l)}$ instead of $\alpha_s^{(n_l+1)}$. It is obtained by using the decoupling relation for α_s which is given by[6]

$$\alpha_s^{(n_l+1)} = \zeta_{\alpha_s} \alpha_s^{(n_l)} \,, \tag{33}$$

with

$$\zeta_{\alpha_s} = 1 + \frac{1}{6}\frac{\alpha_s^{(n_l)}}{\pi} \log\left(\frac{\mu^2}{m^2(\mu^2)}\right) + \mathcal{O}(\alpha_s^2) \,, \tag{34}$$

where results up to four-loop order can be found in Refs. [67, 68]. In our case we only need three-loop corrections which have been computed for the first time in Ref. [69]. Inserting Eq. (33) into the equation for z_m leads to

$$c_m(n_l) = c_m(n_l+1)\big|_{\alpha_s^{(n_l+1)} \to \alpha_s^{(n_l)}} + \delta c_m(n_l) \,, \tag{35}$$

with

$$\delta c_m^{(2)} = \frac{l_\mu^2}{6} + \frac{2 l_\mu}{9} \,, \tag{36}$$

$$\begin{aligned} \delta c_m^{(3)} = \Bigg[& \left(-\frac{\zeta_3}{18} + \frac{\pi^2}{9} + \frac{117}{32} + \frac{1}{27}\pi^2 \log(2) \right) l_\mu + \frac{5 l_\mu^3}{8} + \frac{25 l_\mu^2}{9} \\ & + \left\{ -\frac{l_\mu^3}{36} - \frac{13 l_\mu^2}{108} + \left(-\frac{71}{432} - \frac{\pi^2}{54} \right) l_\mu \right\} n_l - \frac{11}{54} \Bigg] \,, \end{aligned} \tag{37}$$

[6] The formulae of this subsection and the ones of the appendix (except Appendix E) can be found on the website `https://www.ttp.kit.edu/_media/progdata/2016/ttp16-023.tgz`.

$$
\begin{aligned}
\delta c_m^{(4)} = \Bigg[& l_\mu \bigg(-\frac{110a_4}{27} - \frac{1439\pi^2\zeta_3}{864} + \frac{107515\zeta_3}{27648} + \frac{1975\zeta_5}{432} - \frac{695\pi^4}{15552} + \frac{676601\pi^2}{77760} \\
& + \frac{18532949}{373248} - \frac{55\log^4(2)}{324} - \frac{11}{81}\pi^2\log^2(2) - \frac{271}{162}\pi^2\log(2) \bigg) \\
& + n_l \bigg\{ l_\mu \bigg(\frac{4a_4}{27} - \frac{241\zeta_3}{144} + \frac{61\pi^4}{3888} - \frac{1057\pi^2}{1296} - \frac{502145}{93312} + \frac{\log^4(2)}{162} \\
& + \frac{1}{81}\pi^2\log^2(2) - \frac{11}{162}\pi^2\log(2) \bigg) + \bigg(-\frac{7\zeta_3}{18} - \frac{25\pi^2}{108} - \frac{11233}{2592} - \frac{1}{54}\pi^2\log(2) \bigg) l_\mu^2 \\
& - \frac{83l_\mu^4}{432} - \frac{1171l_\mu^3}{864} + \frac{11\pi^2}{648} + \frac{12295}{46656} \bigg\} + \frac{83099\zeta_3}{20736} + \bigg(-\frac{17\zeta_3}{18} + \frac{19\pi^2}{18} + \frac{442177}{10368} \\
& + \frac{19}{54}\pi^2\log(2) \bigg) l_\mu^2 + \frac{431l_\mu^4}{216} + \frac{8869l_\mu^3}{648} + n_l^2 \bigg\{ \bigg(\frac{7\zeta_3}{108} + \frac{13\pi^2}{648} + \frac{2353}{46656} \bigg) l_\mu + \frac{l_\mu^4}{216} \\
& + \frac{13l_\mu^3}{432} + \bigg(\frac{89}{1296} + \frac{\pi^2}{108} \bigg) l_\mu^2 \bigg\} - \frac{11\pi^2}{108} - \frac{209567}{23328} - \frac{11}{324}\pi^2\log(2) \Bigg] ,
\end{aligned}
\tag{38}
$$

with

$$
l_\mu = \log\left(\frac{\mu^2}{m(\mu)^2}\right) , \quad a_n = \mathrm{Li}_n\left(\frac{1}{2}\right) . \tag{39}
$$

5 Conclusions

The main result of this paper is the calculation of the four-loop coefficient in the relation between the $\overline{\mathrm{MS}}$ and on-shell heavy quark mass. Up to the reduction to master integrals the calculation is performed analytically. However, most of the master integrals are only known numerically. For QCD, we managed to obtain an uncertainty of 0.2% for the four-loop coefficient.

We have also computed the coefficients of the individual colour structures. It is interesting to note that the large coefficients (z_m^{FAAA} and z_m^{FAAL}) are known to high precision and furthermore also have large colour factors. Thus, they dominate the numerical result obtained after specifying N_c, in particular the physical result for $N_c = 3$. Some coefficients are known to high relative precision, others have uncertainties of about 30%. There is one coefficient ($z_m^{d_{FA}}$) with an uncertainty which is larger than the central value. Fortunately, it has only a minor numerical contribution to z_m.

In this paper several applications have been discussed. Among them is the numerical analysis of the heavy quark relation for the top, bottom and charm quark. Furthermore, the relations between the $\overline{\mathrm{MS}}$ and several threshold masses are investigated. The numerical results presented in Section 4 are easily reproduced with the help of `RunDec` [40] and `CRunDec` [41] where the latest results for the mass relations are implemented.

Acknowledgements

We are thankful to Tobias Huber for advice on numerical evaluation of MB integrals. We thank the High Performance Computing Center Stuttgart (HLRS) and the Supercomputing Center of Lomonosov Moscow State University [70] for providing computing time used for the numerical computations with `FIESTA`. P.M was supported in part by the EU Network HIGGSTOOLS PITN-GA-2012-316704. The work of V.S. was supported by the Alexander von Humboldt Foundation (Humboldt Forschungspreis).

A Integral families

Graphical representation of the 102 integral families are shown in Figs. 9 to 11. They are obtained from Fig. 2 by introducing a through-going massive line. Note that tables are only required for 100 families since the colour factors of the diagrams mapped to two familes are zero.

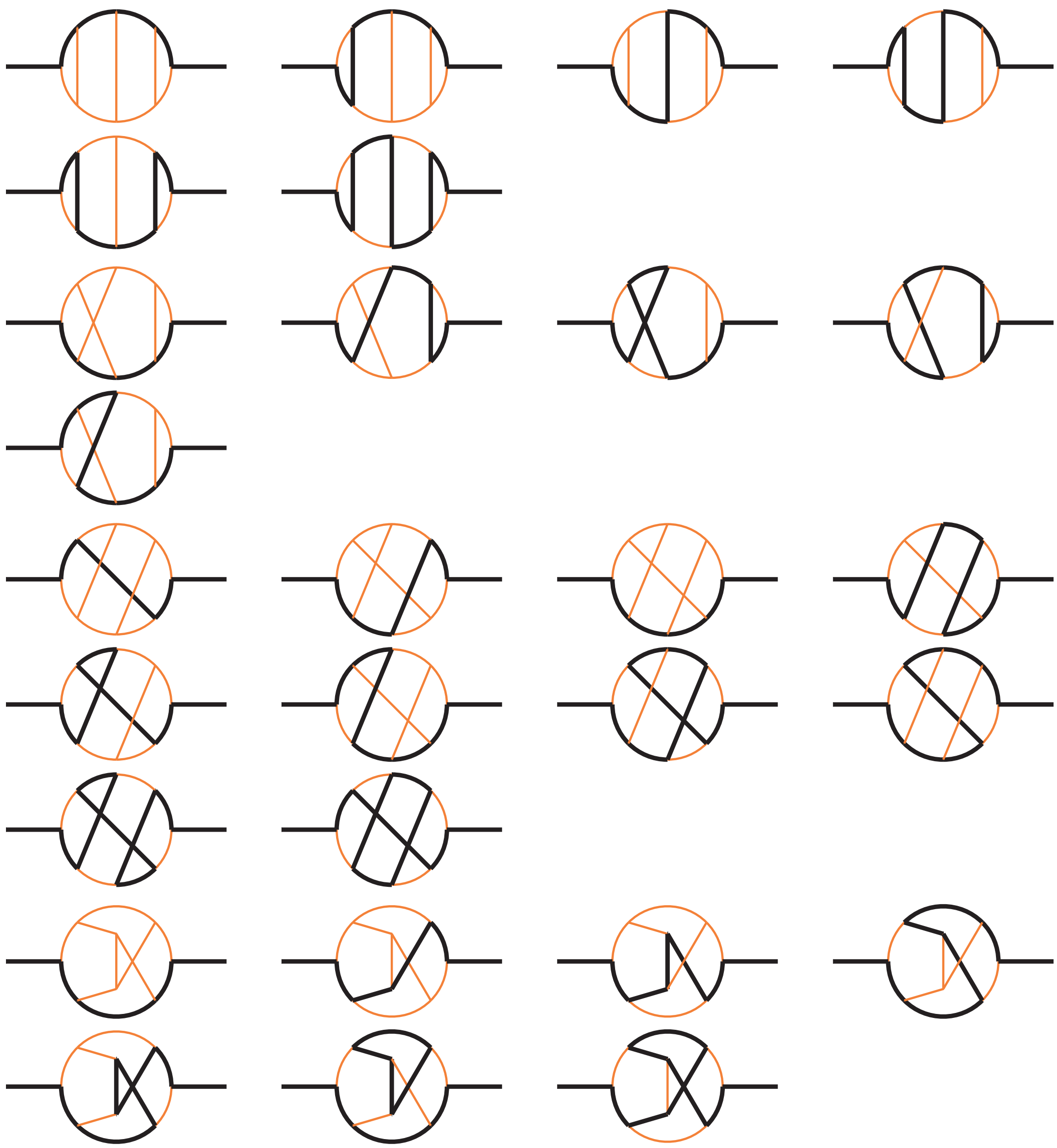

Figure 9: Integral families needed at four-loop order. Thick black lines indicate massive and thin orange lines massless particles.

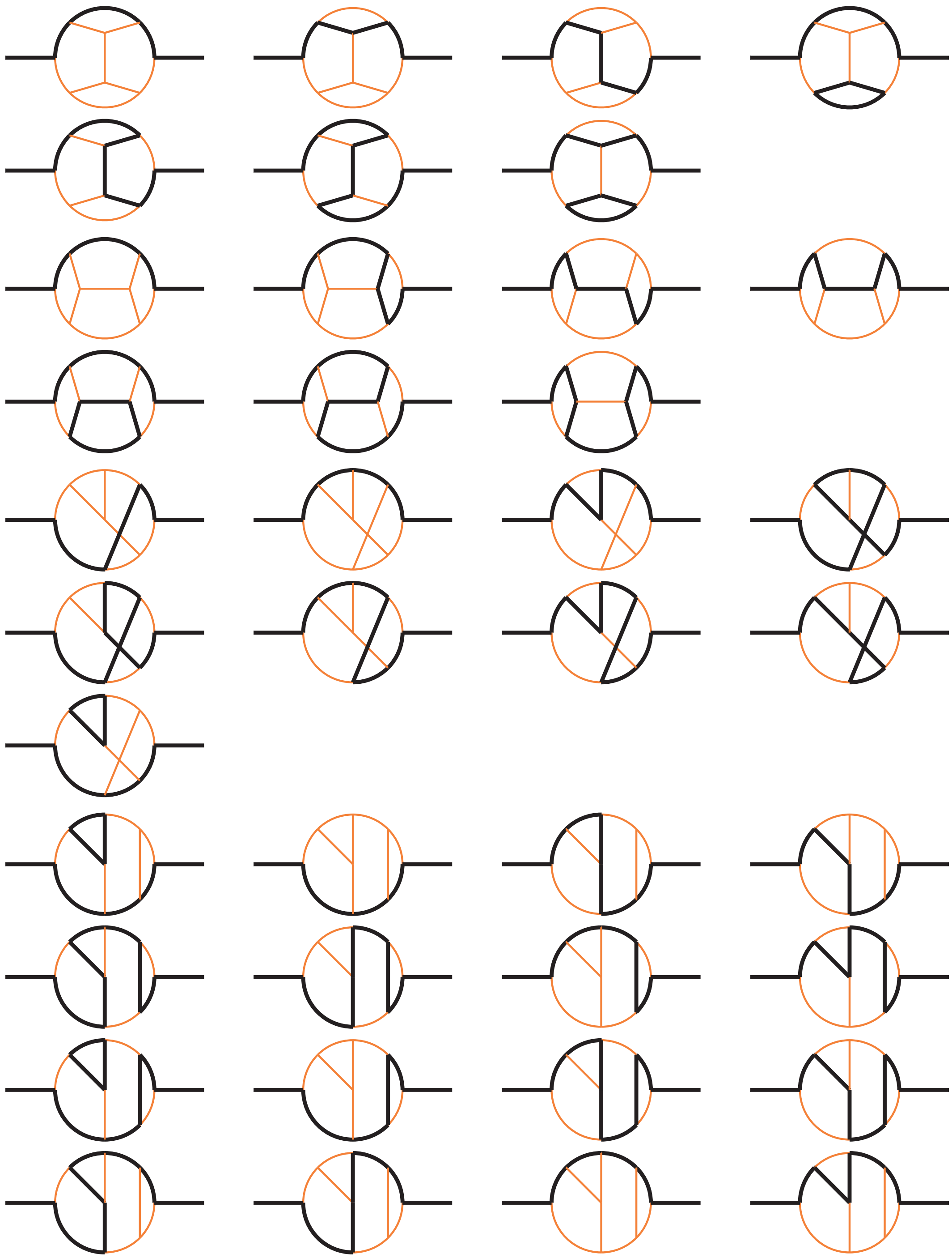

Figure 10: Four-loop families (continued).

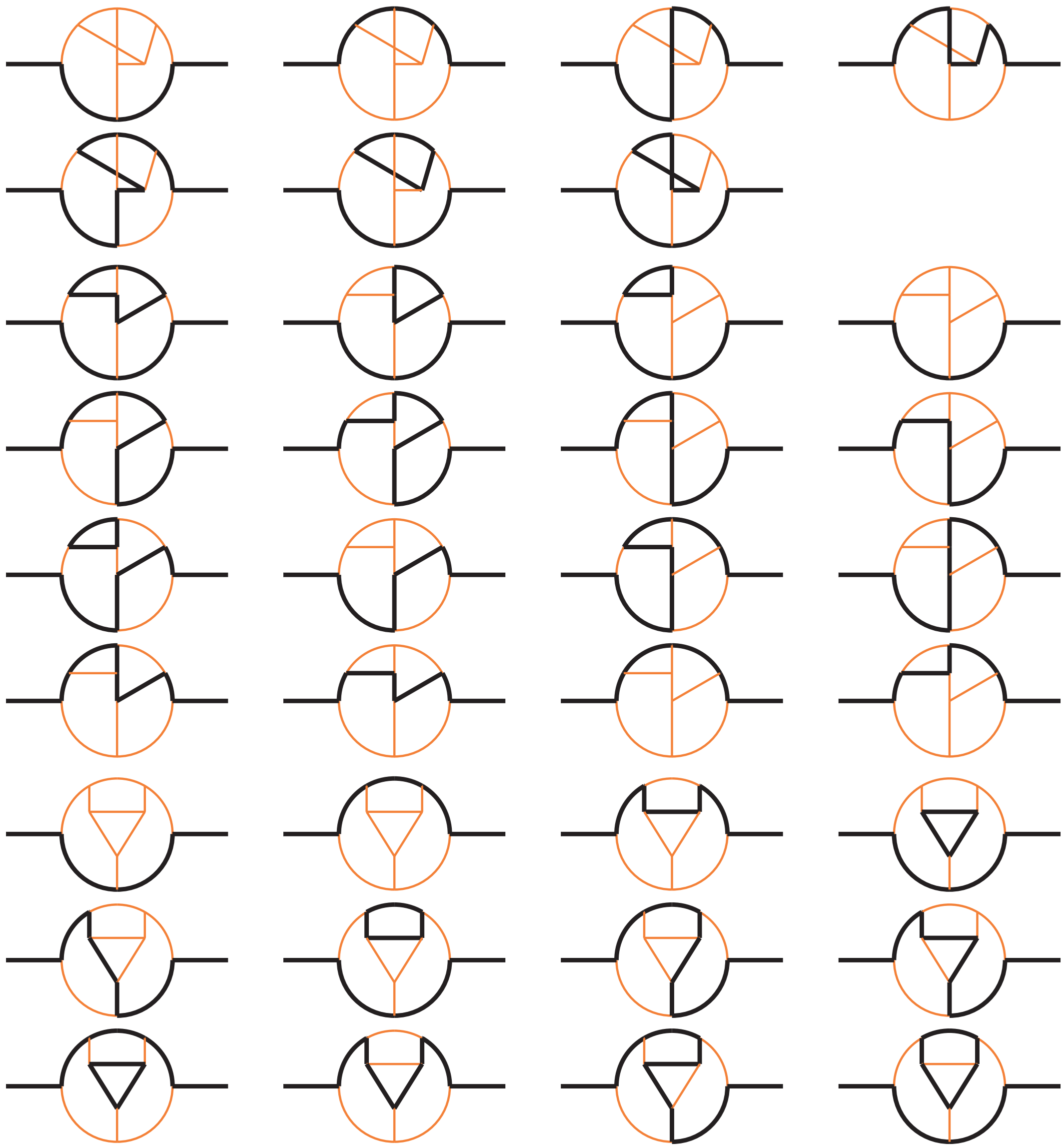

Figure 11: Four-loop families (continued).

B Analytic results for z_m up to three loops

In this Appendix we present analytic results for z_m up to three loops including higher order terms in ϵ which might be important in case the relation between the $\overline{\rm MS}$ and on-shell mass is used in divergent expressions. For $\mu^2 = M^2$ our results read

$$
\begin{aligned}
z_m^{(1)} &= \left(\frac{\zeta(3)}{3} - 8 - \frac{\pi^2}{6} - \frac{3\pi^4}{640}\right)\epsilon^3 C_F + \left(\frac{\zeta(3)}{4} - 4 - \frac{\pi^2}{12}\right)\epsilon^2 C_F \\
&+ \left(-2 - \frac{\pi^2}{16}\right)\epsilon C_F - C_F\,, \\
z_m^{(2)} &= \epsilon\Bigg(C_A C_F\Bigg(6a_4 + \frac{13\zeta_3}{4} - \frac{7\pi^4}{80} + \frac{271\pi^2}{1152} - \frac{8581}{768} + \frac{\log^4(2)}{4} \\
&+ \frac{1}{2}\pi^2\log^2(2) - \frac{3}{2}\pi^2\log(2)\Bigg) + C_F^2\Bigg(-12a_4 - \frac{33\zeta_3}{4} + \frac{7\pi^4}{40} \\
&- \frac{213\pi^2}{128} - \frac{91}{256} - \frac{\log^4(2)}{2} - \pi^2\log^2(2) + 3\pi^2\log(2)\Bigg) \\
&+ TC_F\left(-\frac{7\zeta_3}{2} - \frac{227\pi^2}{288} + \frac{1133}{192} + \pi^2\log(2)\right)n_h + \left(\zeta_3 + \frac{97\pi^2}{288} + \frac{581}{192}\right)TC_F n_l\Bigg) \\
&+ \epsilon^2\Bigg(C_A C_F\Bigg(36a_4 + 36a_5 - \frac{11\pi^2\zeta_3}{16} + \frac{3929\zeta_3}{288} - \frac{609\zeta_5}{16} - \frac{1087\pi^4}{2560} \\
&+ \frac{1537\pi^2}{2304} - \frac{58543}{1536} - \frac{3\log^5(2)}{10} + \frac{3\log^4(2)}{2} - \pi^2\log^3(2) + 3\pi^2\log^2(2) \\
&+ \frac{13}{60}\pi^4\log(2) - \frac{11}{2}\pi^2\log(2)\Bigg) + C_F^2\Bigg(-72a_4 - 72a_5 + \frac{11\pi^2\zeta_3}{8} - \frac{1195\zeta_3}{32} \\
&+ \frac{609\zeta_5}{8} + \frac{5119\pi^4}{7680} - \frac{1639\pi^2}{256} - \frac{1905}{512} + \frac{3\log^5(2)}{5} - 3\log^4(2) + 2\pi^2\log^3(2) \\
&- 6\pi^2\log^2(2) - \frac{13}{30}\pi^4\log(2) + 11\pi^2\log(2)\Bigg) + TC_F n_h\Bigg(-24a_4 - \frac{1273\zeta_3}{72} \\
&+ \frac{93\pi^4}{640} - \frac{1553\pi^2}{576} + \frac{8135}{384} - \log^4(2) - 2\pi^2\log^2(2) + 5\pi^2\log(2)\Bigg) \\
&+ \left(\frac{239\zeta_3}{72} + \frac{199\pi^4}{1920} + \frac{643\pi^2}{576} + \frac{4079}{384}\right)TC_F n_l\Bigg) \\
&+ C_A C_F\left(\frac{3\zeta_3}{8} + \frac{\pi^2}{12} - \frac{1111}{384} - \frac{1}{4}\pi^2\log(2)\right) \\
&+ C_F^2\left(-\frac{3\zeta_3}{4} - \frac{5\pi^2}{16} + \frac{7}{128} + \frac{1}{2}\pi^2\log(2)\right) \\
&+ \left(\frac{143}{96} - \frac{\pi^2}{6}\right)TC_F n_h + \left(\frac{71}{96} + \frac{\pi^2}{12}\right)TC_F n_l\,,
\end{aligned}
$$

$$
\begin{aligned}
z_m^{(3)} = {} & C_A {C_F}^2 \Bigg(-\frac{4a_4}{3} - \frac{19\pi^2\zeta_3}{16} - \frac{773\zeta_3}{96} + \frac{45\zeta_5}{16} + \frac{65\pi^4}{432} + \frac{509\pi^2}{576} + \frac{13189}{4608} \\
& - \frac{\log^4(2)}{18} - \frac{31}{36}\pi^2\log^2(2) - \frac{31}{72}\pi^2\log(2) \Bigg) + {C_A}^2 C_F \Bigg(\frac{11a_4}{3} + \frac{51\pi^2\zeta_3}{64} + \frac{1343\zeta_3}{288} \\
& - \frac{65\zeta_5}{32} - \frac{179\pi^4}{3456} - \frac{1955\pi^2}{3456} - \frac{1322545}{124416} + \frac{11\log^4(2)}{72} + \frac{11}{36}\pi^2\log^2(2) - \frac{115}{72}\pi^2\log(2) \Bigg) \\
& + T n_h \Bigg(C_A C_F \Bigg(-\frac{4a_4}{3} + \frac{\pi^2\zeta_3}{8} - \frac{109\zeta_3}{144} - \frac{5\zeta_5}{8} - \frac{43\pi^4}{1080} - \frac{449\pi^2}{144} + \frac{144959}{15552} - \frac{\log^4(2)}{18} \\
& + \frac{1}{18}\pi^2\log^2(2) + \frac{32}{9}\pi^2\log(2) \Bigg) + {C_F}^2 \Bigg(\frac{8a_4}{3} - \frac{53\zeta_3}{24} + \frac{91\pi^4}{2160} - \frac{85\pi^2}{108} + \frac{1067}{576} + \frac{\log^4(2)}{9} \\
& - \frac{1}{9}\pi^2\log^2(2) + \frac{8}{9}\pi^2\log(2) \Bigg) \Bigg) + T n_l \Bigg(C_A C_F \Bigg(-\frac{4a_4}{3} + \frac{89\zeta_3}{144} + \frac{19\pi^4}{2160} + \frac{175\pi^2}{432} \\
& + \frac{70763}{15552} - \frac{\log^4(2)}{18} - \frac{1}{9}\pi^2\log^2(2) + \frac{11}{18}\pi^2\log(2) \Bigg) + {C_F}^2 \Bigg(\frac{8a_4}{3} + \frac{55\zeta_3}{24} - \frac{119\pi^4}{2160} \\
& + \frac{13\pi^2}{18} + \frac{1283}{576} + \frac{\log^4(2)}{9} + \frac{2}{9}\pi^2\log^2(2) - \frac{11}{9}\pi^2\log(2) \Bigg) \Bigg) + {C_F}^3 \Bigg(-12a_4 - \frac{\pi^2\zeta_3}{16} \\
& - \frac{81\zeta_3}{16} + \frac{5\zeta_5}{8} - \frac{\pi^4}{48} - \frac{613\pi^2}{192} - \frac{2969}{768} - \frac{\log^4(2)}{2} + \frac{1}{2}\pi^2\log^2(2) + \frac{29}{4}\pi^2\log(2) \Bigg) \\
& + \left(\frac{2\zeta_3}{9} + \frac{13\pi^2}{108} - \frac{5917}{3888} \right) T^2 C_F n_h n_l + \left(\frac{11\zeta_3}{18} + \frac{4\pi^2}{135} - \frac{9481}{7776} \right) T^2 C_F {n_h}^2 \\
& + \left(-\frac{7\zeta_3}{18} - \frac{13\pi^2}{108} - \frac{2353}{7776} \right) T^2 C_F {n_l}^2 \\
& + \epsilon \Bigg\{ \Bigg(-\frac{{\zeta_3}^2}{2} + \frac{21}{8}\pi^2\log(2)\zeta_3 + \frac{1621\pi^2\zeta_3}{192} - \frac{1761\zeta_3}{16} - 300a_4 + \frac{103\zeta_5}{4} - 72a_5 \\
& + \frac{3\log^5(2)}{5} + \frac{1}{8}\pi^2\log^4(2) - \frac{25\log^4(2)}{2} - \pi^2\log^3(2) - \frac{1}{8}\pi^4\log^2(2) - \frac{93}{4}\pi^2\log^2(2) \\
& - \frac{141}{160}\pi^4\log(2) + \frac{317}{4}\pi^2\log(2) - \frac{5\pi^6}{189} + \frac{437\pi^4}{1280} + 3a_4\pi^2 - \frac{110185\pi^2}{6144} - \frac{15709}{512} \Bigg) {C_F}^3 \\
& + C_A \Bigg(-\frac{249{\zeta_3}^2}{16} + 7\pi^2\log(2)\zeta_3 - \frac{3125\pi^2\zeta_3}{384} - \frac{767\zeta_3}{36} + \frac{34a_4}{9} + \frac{5935\zeta_5}{48} - \frac{200a_5}{3} \\
& + \frac{5\log^5(2)}{9} + \frac{1}{3}\pi^2\log^4(2) + \frac{17\log^4(2)}{108} + \frac{181}{54}\pi^2\log^3(2) - \frac{1}{3}\pi^4\log^2(2) \\
& - \frac{4765}{216}\pi^2\log^2(2) + \frac{911\pi^4\log(2)}{1728} - \frac{1181}{54}\pi^2\log(2) - \frac{7709\pi^6}{60480} + \frac{10219\pi^4}{3240} + 8a_4\pi^2 \\
& - \frac{174769\pi^2}{55296} + \frac{339421}{27648} \Bigg) {C_F}^2 + {n_l}^2 T^2 \Bigg(-\frac{197\zeta_3}{54} - \frac{23\pi^4}{270} - \frac{679\pi^2}{864} - \frac{131425}{46656} \Bigg) C_F \\
& + {n_h}^2 T^2 \Bigg(\frac{16a_4}{3} + \frac{1247\zeta_3}{270} + \frac{2\log^4(2)}{9} - \frac{2}{9}\pi^2\log^2(2) - \frac{8}{45}\pi^2\log(2) - \frac{31\pi^4}{1080}
\end{aligned}
$$

$$
\begin{aligned}
&+\frac{5803\pi^2}{7200}-\frac{2404781}{233280}\bigg)C_F+n_hn_lT^2\bigg(\frac{16a_4}{3}+\frac{163\zeta_3}{27}+\frac{2\log^4(2)}{9}+\frac{4}{9}\pi^2\log^2(2)\\
&-\frac{16}{9}\pi^2\log(2)+\frac{5\pi^4}{72}+\frac{289\pi^2}{432}-\frac{314485}{23328}\bigg)C_F+{C_A}^2\bigg(\frac{137{\zeta_3}^2}{16}-\frac{133}{32}\pi^2\log(2)\zeta_3\\
&+\frac{43\pi^2\zeta_3}{48}+\frac{7433\zeta_3}{432}+\frac{658a_4}{9}-\frac{2939\zeta_5}{48}+\frac{154a_5}{3}-\frac{77\log^5(2)}{180}-\frac{19}{96}\pi^2\log^4(2)\\
&+\frac{329\log^4(2)}{108}-\frac{77}{54}\pi^2\log^3(2)+\frac{19}{96}\pi^4\log^2(2)+\frac{1819}{108}\pi^2\log^2(2)-\frac{187\pi^4\log(2)}{4320}\\
&-\frac{3835}{432}\pi^2\log(2)+\frac{9469\pi^6}{120960}-\frac{31319\pi^4}{20736}-\frac{19a_4\pi^2}{4}-\frac{17873\pi^2}{6912}-\frac{52167985}{746496}\bigg)C_F\\
&+n_hT\bigg(\bigg(-\frac{328a_4}{9}-\frac{211\pi^2\zeta_3}{48}-\frac{499\zeta_3}{18}+\frac{28\zeta_5}{3}+16a_5-\frac{2\log^5(2)}{15}-\frac{41\log^4(2)}{27}\\
&+\frac{2}{9}\pi^2\log^3(2)-\frac{175}{27}\pi^2\log^2(2)+\frac{29}{180}\pi^4\log(2)+\frac{1151}{54}\pi^2\log(2)+\frac{5393\pi^4}{12960}\\
&-\frac{136901\pi^2}{13824}+\frac{19129}{1152}\bigg){C_F}^2+C_A\bigg(\frac{19{\zeta_3}^2}{8}+\frac{21}{8}\pi^2\log(2)\zeta_3+\frac{41\pi^2\zeta_3}{12}-\frac{44381\zeta_3}{432}\\
&-\frac{1228a_4}{9}-\frac{143\zeta_5}{12}-8a_5+\frac{\log^5(2)}{15}+\frac{1}{8}\pi^2\log^4(2)-\frac{307\log^4(2)}{54}-\frac{1}{9}\pi^2\log^3(2)\\
&-\frac{1}{8}\pi^4\log^2(2)-\frac{697}{27}\pi^2\log^2(2)-\frac{29}{360}\pi^4\log(2)+\frac{2147}{54}\pi^2\log(2)-\frac{41\pi^6}{1080}\\
&+\frac{18151\pi^4}{25920}+3a_4\pi^2-\frac{8677\pi^2}{864}+\frac{6253805}{93312}\bigg)C_F\bigg)+n_lT\bigg(\bigg(\frac{496a_4}{9}-\frac{73\pi^2\zeta_3}{48}\\
&+\frac{491\zeta_3}{18}-\frac{131\zeta_5}{3}+\frac{112a_5}{3}-\frac{14\log^5(2)}{45}+\frac{62\log^4(2)}{27}-\frac{28}{27}\pi^2\log^3(2)\\
&+\frac{124}{27}\pi^2\log^2(2)-\frac{17}{540}\pi^4\log(2)-\frac{256}{27}\pi^2\log(2)-\frac{11527\pi^4}{25920}+\frac{89507\pi^2}{13824}+\frac{54083}{3456}\bigg){C_F}^2\\
&+C_A\bigg(-\frac{248a_4}{9}+\frac{13\pi^2\zeta_3}{24}+\frac{2329\zeta_3}{432}+\frac{455\zeta_5}{24}-\frac{56a_5}{3}+\frac{7\log^5(2)}{45}-\frac{31\log^4(2)}{27}\\
&+\frac{14}{27}\pi^2\log^3(2)-\frac{62}{27}\pi^2\log^2(2)+\frac{17\pi^4\log(2)}{1080}+\frac{128}{27}\pi^2\log(2)\\
&+\frac{11297\pi^4}{25920}+\frac{2587\pi^2}{864}+\frac{2963153}{93312}\bigg)C_F\bigg)\bigg\}\,,
\end{aligned}
$$

with

$$
a_4=\mathrm{Li}_4\left(\frac{1}{2}\right)\,.
$$

The logarithmic contributions can be found in Appendix C.

C Renormalization scale dependence of $z_m^{(4)}$

In this Appendix we present the dependence of $z_m(\mu)$ and $c_m(\mu)$ on $\log(\mu)$. The corresponding analytic expressions are easily constructed from Eqs. (10) and (13) by taking the derivative with respect to μ^2 and exploiting the fact that M is μ-independent. The μ-dependence of $m(\mu)$ and $\alpha_s(\mu)$ is governed by corresponding renormalization group equations which are needed to four- and three-loop accuracy, respectively.

Our results read

$$z_m^{(1),\log} = -\frac{3}{4}C_F L_M\,, \tag{40}$$

$$\begin{aligned}
z_m^{(2),\log} &= L_M\Bigg(-\frac{185C_AC_F}{96}+\frac{13}{24}TC_Fn_h+\frac{13}{24}TC_Fn_l+\frac{21C_F^2}{32}\Bigg)\\
&+L_M^2\Bigg\{-\frac{11C_AC_F}{32}+\frac{1}{8}TC_Fn_h+\frac{1}{8}TC_Fn_l+\frac{9C_F^2}{32}\Bigg\}\,,
\end{aligned} \tag{41}$$

$$\begin{aligned}
z_m^{(3),\log} &= L_M\Bigg\{Tn_h\Bigg(C_AC_F\Bigg(\frac{\zeta_3}{2}+\frac{\pi^2l_2}{6}-\frac{13\pi^2}{36}+\frac{583}{108}\Bigg)\\
&+C_F^2\Bigg(-\frac{\zeta_3}{4}-\frac{1}{3}\pi^2l_2+\frac{\pi^2}{3}-\frac{151}{384}\Bigg)\Bigg)+C_AC_F^2\Bigg(-\frac{53\zeta_3}{32}+\frac{53\pi^2l_2}{48}-\frac{61\pi^2}{96}+\frac{5813}{1536}\Bigg)\\
&+C_A^2C_F\Bigg(\frac{11\zeta_3}{16}-\frac{11}{24}\pi^2l_2+\frac{11\pi^2}{72}-\frac{13243}{1728}\Bigg)+Tn_l\Bigg(C_AC_F\Bigg(\frac{\zeta_3}{2}+\frac{\pi^2l_2}{6}+\frac{7\pi^2}{72}+\frac{869}{216}\Bigg)\\
&+C_F^2\Bigg(-\frac{\zeta_3}{4}-\frac{1}{3}\pi^2l_2+\frac{7\pi^2}{48}+\frac{65}{384}\Bigg)\Bigg)+\Bigg(\frac{\pi^2}{18}-\frac{143}{108}\Bigg)T^2C_Fn_hn_l\\
&+\Bigg(\frac{\pi^2}{9}-\frac{197}{216}\Bigg)T^2C_Fn_h^2+C_F^3\Bigg(\frac{9\zeta_3}{16}-\frac{3}{8}\pi^2l_2+\frac{15\pi^2}{64}-\frac{489}{512}\Bigg)+\Bigg(-\frac{89}{216}-\frac{\pi^2}{18}\Bigg)T^2C_Fn_l^2\Bigg\}\\
&+L_M^2\Bigg\{Tn_h\Bigg(\frac{373C_AC_F}{288}-\frac{13C_F^2}{32}\Bigg)+Tn_l\Bigg(\frac{373C_AC_F}{288}-\frac{13C_F^2}{32}\Bigg)+\frac{109}{64}C_AC_F^2\\
&-\frac{2341C_A^2C_F}{1152}-\frac{13}{36}T^2C_Fn_hn_l-\frac{13}{72}T^2C_Fn_h^2-\frac{13}{72}T^2C_Fn_l^2-\frac{27C_F^3}{128}\Bigg\}\\
&+L_M^3\Bigg\{Tn_h\Bigg(\frac{11C_AC_F}{72}-\frac{3C_F^2}{32}\Bigg)+Tn_l\Bigg(\frac{11C_AC_F}{72}-\frac{3C_F^2}{32}\Bigg)+\frac{33}{128}C_AC_F^2\\
&-\frac{121}{576}C_A^2C_F-\frac{1}{18}T^2C_Fn_hn_l-\frac{1}{36}T^2C_Fn_h^2-\frac{1}{36}T^2C_Fn_l^2-\frac{9C_F^3}{128}\Bigg\}\,,
\end{aligned} \tag{42}$$

$$\begin{aligned}
z_m^{(4),\log} &= L_M\Bigg\{\Bigg(\frac{3{l_2}^4}{8}-\frac{3}{8}\pi^2{l_2}^2-\frac{351\pi^2l_2}{64}+9a_4+\frac{3\pi^2\zeta_3}{64}+\frac{663\zeta_3}{128}\\
&-\frac{15\zeta_5}{32}+\frac{\pi^4}{64}+\frac{1241\pi^2}{512}+\frac{18505}{4096}\Bigg){C_F}^4+C_A\Bigg(-\frac{4{l_2}^4}{3}+\frac{97}{48}\pi^2{l_2}^2\\
&+\frac{7595\pi^2l_2}{384}-32a_4+\frac{23\pi^2\zeta_3}{32}-\frac{2149\zeta_3}{256}-\frac{25\zeta_5}{64}-\frac{49\pi^4}{288}-\frac{4677\pi^2}{512}-\frac{55487}{3072}\Bigg){C_F}^3
\end{aligned}$$

$$
\begin{aligned}
&+ {C_A}^2\Bigg(- \frac{77{l_2}^4}{288} - \frac{187}{72}\pi^2{l_2}^2 + \frac{1123\pi^2 l_2}{1152} - \frac{77a_4}{12} - \frac{989\pi^2\zeta_3}{256} - \frac{6781\zeta_3}{256} + \frac{965\zeta_5}{128} \\
&+ \frac{6257\pi^4}{13824} + \frac{3575\pi^2}{1536} + \frac{8025563}{331776}\Bigg){C_F}^2 + \frac{2489 n_h {n_l}^2 T^3 C_F}{1296} \\
&+ {n_h}^2 n_l T^3\Bigg(- \zeta_3 - \frac{3\pi^2}{20} + \frac{3677}{1296}\Bigg)C_F + {n_h}^3 T^3\Bigg(- \frac{2\zeta_3}{3} - \frac{4\pi^2}{135} + \frac{4865}{3888}\Bigg)C_F \\
&+ {n_l}^3 T^3\Bigg(\frac{\zeta_3}{3} + \frac{13\pi^2}{108} + \frac{1301}{3888}\Bigg)C_F + {C_A}^3\Bigg(\frac{121{l_2}^4}{288} + \frac{121}{144}\pi^2{l_2}^2 - \frac{1367\pi^2 l_2}{288} \\
&+ \frac{121a_4}{12} + \frac{561\pi^2\zeta_3}{256} + \frac{1223\zeta_3}{96} - \frac{495\zeta_5}{128} - \frac{1969\pi^4}{13824} - \frac{19873\pi^2}{13824} - \frac{4722671}{124416}\Bigg)C_F \\
&- \frac{d_{FF} n_h}{4N_c} - \frac{d_{FF} n_l}{4N_c} + \frac{15 d_{FF} n_h \zeta_3}{8N_c} + \frac{15 d_{FF} n_l \zeta_3}{8N_c} - \frac{15 d_{FA}\zeta_3}{16N_c} + \frac{d_{FA}}{8N_c} \\
&+ {n_l}^2 T^2\Bigg(\Bigg(- \frac{{l_2}^4}{9} - \frac{2}{9}\pi^2{l_2}^2 + \frac{11\pi^2 l_2}{9} - \frac{8a_4}{3} - \frac{11\zeta_3}{8} + \frac{11\pi^4}{216} - \frac{21\pi^2}{32} - \frac{50131}{20736}\Bigg){C_F}^2 \\
&+ C_A\Bigg(\frac{{l_2}^4}{18} + \frac{1}{9}\pi^2{l_2}^2 - \frac{11\pi^2 l_2}{18} + \frac{4a_4}{3} - \frac{37\zeta_3}{16} - \frac{\pi^4}{216} - \frac{29\pi^2}{36} - \frac{15953}{2592}\Bigg)C_F\Bigg) \\
&+ n_h n_l T^2\Bigg(\Bigg(- \frac{2{l_2}^4}{9} - \frac{1}{9}\pi^2{l_2}^2 + \frac{\pi^2 l_2}{3} - \frac{16a_4}{3} + \zeta_3 + \frac{\pi^4}{216} - \frac{\pi^2}{864} - \frac{41383}{10368}\Bigg){C_F}^2 \\
&+ C_A\Bigg(\frac{{l_2}^4}{9} + \frac{1}{18}\pi^2{l_2}^2 - \frac{25\pi^2 l_2}{6} + \frac{8a_4}{3} - \frac{\pi^2\zeta_3}{8} - \frac{\zeta_3}{2} + \frac{5\zeta_5}{8} + \frac{17\pi^4}{432} \\
&+ \frac{1345\pi^2}{432} - \frac{26213}{1296}\Bigg)C_F\Bigg) + {n_h}^2 T^2\Bigg(\Bigg(- \frac{{l_2}^4}{9} + \frac{1}{9}\pi^2{l_2}^2 - \frac{8\pi^2 l_2}{9} - \frac{8a_4}{3} + \frac{19\zeta_3}{8} \\
&- \frac{5\pi^4}{108} + \frac{1757\pi^2}{2160} - \frac{32635}{20736}\Bigg){C_F}^2 + C_A\Bigg(\frac{{l_2}^4}{18} - \frac{1}{18}\pi^2{l_2}^2 - \frac{32\pi^2 l_2}{9} + \frac{4a_4}{3} - \frac{\pi^2\zeta_3}{8} \\
&+ \frac{29\zeta_3}{16} + \frac{5\zeta_5}{8} + \frac{19\pi^4}{432} + \frac{7211\pi^2}{2160} - \frac{36473}{2592}\Bigg)C_F\Bigg) + n_l T\Bigg(\Bigg(\frac{5{l_2}^4}{12} - \frac{2}{3}\pi^2{l_2}^2 \\
&- \frac{311\pi^2 l_2}{48} + 10a_4 + \frac{\pi^2\zeta_3}{16} + \frac{69\zeta_3}{32} + \frac{5\zeta_5}{4} + \frac{179\pi^4}{2880} + \frac{175\pi^2}{64} + \frac{883}{512}\Bigg){C_F}^3 \\
&+ C_A\Bigg(\frac{29{l_2}^4}{72} + \frac{14}{9}\pi^2{l_2}^2 - \frac{1075\pi^2 l_2}{288} + \frac{29a_4}{3} + \frac{19\pi^2\zeta_3}{16} + \frac{391\zeta_3}{32} - \frac{25\zeta_5}{8} \\
&- \frac{2567\pi^4}{8640} + \frac{365\pi^2}{384} + \frac{12563}{10368}\Bigg){C_F}^2 + {C_A}^2\Bigg(- \frac{11{l_2}^4}{36} - \frac{11}{18}\pi^2{l_2}^2 + \frac{251\pi^2 l_2}{72} \\
&- \frac{22a_4}{3} - \frac{51\pi^2\zeta_3}{64} + \frac{7\zeta_3}{32} + \frac{15\zeta_5}{32} + \frac{223\pi^4}{3456} + \frac{1991\pi^2}{1152} + \frac{601319}{20736}\Bigg)C_F\Bigg) \\
&+ n_h T\Bigg(\Bigg(\frac{5{l_2}^4}{12} - \frac{5}{12}\pi^2{l_2}^2 - \frac{129\pi^2 l_2}{16} + 10a_4 + \frac{\pi^2\zeta_3}{16} + \frac{177\zeta_3}{32} + \frac{5\zeta_5}{4} \\
&- \frac{31\pi^4}{2880} + \frac{4481\pi^2}{1152} + \frac{991}{512}\Bigg){C_F}^3 + C_A\Bigg(\frac{29{l_2}^4}{72} + \frac{37}{72}\pi^2{l_2}^2 - \frac{13\pi^2 l_2}{96}
\end{aligned}
$$

$$
\begin{aligned}
&+\frac{29a_4}{3}+\frac{35\pi^2\zeta_3}{32}+\frac{7\zeta_3}{8}-\frac{85\zeta_5}{32}+\frac{29\pi^4}{4320}-\frac{527\pi^2}{1728}-\frac{10771}{2592}\bigg){C_F}^2\\
&+{C_A}^2\bigg(-\frac{11{l_2}^4}{36}-\frac{11}{72}\pi^2{l_2}^2+\frac{139\pi^2 l_2}{12}-\frac{22a_4}{3}-\frac{29\pi^2\zeta_3}{64}-\frac{57\zeta_3}{16}-\frac{5\zeta_5}{4}\\
&-\frac{239\pi^4}{3456}-\frac{28735\pi^2}{3456}+\frac{895403}{20736}\bigg)C_F\bigg)\bigg\}\\
&+L_M^2\bigg\{T^2n_h^2\bigg(C_AC_F\bigg(-\frac{\zeta_3}{4}-\frac{1}{12}\pi^2l_2+\frac{\pi^2}{3}-\frac{9707}{2304}\bigg)+C_F^2\bigg(\frac{\zeta_3}{8}+\frac{\pi^2l_2}{6}\\
&-\frac{5\pi^2}{24}+\frac{923}{2304}\bigg)\bigg)+T^2n_hn_l\bigg(C_AC_F\bigg(-\frac{\zeta_3}{2}-\frac{1}{6}\pi^2l_2+\frac{5\pi^2}{24}-\frac{8123}{1152}\bigg)\\
&+C_F^2\bigg(\frac{\zeta_3}{4}+\frac{\pi^2l_2}{3}-\frac{25\pi^2}{96}+\frac{383}{1152}\bigg)\bigg)+Tn_h\bigg(C_AC_F^2\bigg(\frac{\zeta_3}{64}-\frac{103}{96}\pi^2l_2\\
&+\frac{175\pi^2}{192}-\frac{10853}{2304}\bigg)+C_A^2C_F\bigg(\frac{11\zeta_3}{32}+\frac{11\pi^2l_2}{24}-\frac{55\pi^2}{96}+\frac{6527}{512}\bigg)\\
&+C_F^3\bigg(\frac{3\zeta_3}{32}+\frac{5\pi^2l_2}{16}-\frac{31\pi^2}{128}+\frac{57}{256}\bigg)\bigg)+C_AC_F^3\bigg(\frac{357\zeta_3}{256}-\frac{119}{128}\pi^2l_2\\
&+\frac{287\pi^2}{512}-\frac{6477}{2048}\bigg)+C_A^2C_F^2\bigg(-\frac{649\zeta_3}{256}+\frac{649\pi^2l_2}{384}-\frac{715\pi^2}{768}+\frac{373625}{36864}\bigg)\\
&+C_A^3C_F\bigg(\frac{121\zeta_3}{128}-\frac{121}{192}\pi^2l_2+\frac{121\pi^2}{576}-\frac{337657}{27648}\bigg)+\\
&T^2n_l^2\bigg(C_AC_F\bigg(-\frac{\zeta_3}{4}-\frac{1}{12}\pi^2l_2-\frac{\pi^2}{8}-\frac{6539}{2304}\bigg)+C_F^2\bigg(\frac{\zeta_3}{8}+\frac{\pi^2l_2}{6}-\frac{5\pi^2}{96}-\frac{157}{2304}\bigg)\bigg)\\
&+Tn_l\bigg(C_AC_F^2\bigg(\frac{\zeta_3}{64}-\frac{103}{96}\pi^2l_2+\frac{185\pi^2}{384}-\frac{7883}{2304}\bigg)\\
&+C_A^2C_F\bigg(\frac{11\zeta_3}{32}+\frac{11\pi^2l_2}{24}+\frac{11\pi^2}{192}+\frac{5559}{512}\bigg)+C_F^3\bigg(\frac{3\zeta_3}{32}+\frac{5\pi^2l_2}{16}-\frac{11\pi^2}{64}+\frac{3}{256}\bigg)\bigg)\\
&+\frac{125}{144}T^3C_Fn_hn_l^2+\bigg(\frac{161}{144}-\frac{\pi^2}{12}\bigg)T^3C_Fn_h^2n_l+\bigg(\frac{197}{432}-\frac{\pi^2}{18}\bigg)T^3C_Fn_h^3\\
&+C_F^4\bigg(-\frac{27\zeta_3}{128}+\frac{9\pi^2l_2}{64}-\frac{45\pi^2}{512}+\frac{2889}{4096}\bigg)+\bigg(\frac{89}{432}+\frac{\pi^2}{36}\bigg)T^3C_Fn_l^3\bigg\}\\
&+L_M^3\bigg\{T^2n_hn_l\bigg(\frac{97C_F^2}{288}-\frac{91C_AC_F}{72}\bigg)+T^2n_h^2\bigg(\frac{97C_F^2}{576}-\frac{91C_AC_F}{144}\bigg)\\
&+Tn_h\bigg(-\frac{389}{288}C_AC_F^2+\frac{1163}{576}C_A^2C_F+\frac{9C_F^3}{64}\bigg)+T^2n_l^2\bigg(\frac{97C_F^2}{576}-\frac{91C_AC_F}{144}\bigg)\\
&+Tn_l\bigg(-\frac{389}{288}C_AC_F^2+\frac{1163}{576}C_A^2C_F+\frac{9C_F^3}{64}\bigg)-\frac{45}{64}C_AC_F^3+\frac{21361C_A^2C_F^2}{9216}\\
&-\frac{27995C_A^3C_F}{13824}+\frac{13}{72}T^3C_Fn_hn_l^2+\frac{13}{72}T^3C_Fn_h^2n_l
\end{aligned}
$$

$$
\begin{aligned}
&+\frac{13}{216}T^3C_Fn_h^3+\frac{13}{216}T^3C_Fn_l^3+\frac{45C_F^4}{1024}\Bigg\}\\
&+L_M^4\Bigg\{T^2n_hn_l\left(\frac{11C_F^2}{192}-\frac{11C_AC_F}{96}\right)+T^2n_h^2\left(\frac{11C_F^2}{384}-\frac{11C_AC_F}{192}\right)\\
&+Tn_h\left(-\frac{121}{768}C_AC_F^2+\frac{121}{768}C_A^2C_F+\frac{9C_F^3}{256}\right)+T^2n_l^2\left(\frac{11C_F^2}{384}-\frac{11C_AC_F}{192}\right)\\
&+Tn_l\left(-\frac{121}{768}C_AC_F^2+\frac{121}{768}C_A^2C_F+\frac{9C_F^3}{256}\right)-\frac{99C_AC_F^3}{1024}+\frac{1331C_A^2C_F^2}{6144}\\
&-\frac{1331C_A^3C_F}{9216}+\frac{1}{48}T^3C_Fn_hn_l^2+\frac{1}{48}T^3C_Fn_h^2n_l+\frac{1}{144}T^3C_Fn_h^3\\
&+\frac{1}{144}T^3C_Fn_l^3+\frac{27C_F^4}{2048}\Bigg\}\,,
\end{aligned}
\tag{43}
$$

with

$$
d_{FF}=d_F^{abcd}d_F^{abcd},\; d_{FA}=d_F^{abcd}d_A^{abcd},\; L_M=\log\left(\frac{\mu^2}{M^2}\right),\, l_2=\log(2)\,. \tag{44}
$$

We present the μ dependence of the four-loop term of the inverted relation in the form

$$
c_m^{(4),\log} \;=\; -z_m^{(4),\log}|_{L_M\to l_m}+\delta c_m^{(4),\log}\,, \tag{45}
$$

where

$$
\begin{aligned}
\delta c_m^{(4),\log}&=l_m\Bigg(Tn_h\Bigg(C_AC_F^2\Bigg(2a_4-\frac{3\pi^2\zeta_3}{16}+\frac{89\zeta_3}{48}+\frac{15\zeta_5}{16}+\frac{l_2^4}{12}-\frac{1}{12}\pi^2l_2^2\\
&-\frac{85\pi^2l_2}{16}+\frac{43\pi^4}{720}+\frac{43\pi^2}{9}-\frac{95551}{20736}\Bigg)+C_F^3\Bigg(-4a_4+\frac{21\zeta_3}{8}-\frac{l_2^4}{6}+\frac{1}{6}\pi^2l_2^2\\
&-\frac{11\pi^2l_2}{8}-\frac{91\pi^4}{1440}+\frac{641\pi^2}{576}-\frac{917}{384}\Bigg)\Bigg)+C_AC_F^3\Bigg(2a_4+\frac{57\pi^2\zeta_3}{32}+\frac{1635\zeta_3}{128}\\
&-\frac{135\zeta_5}{32}+\frac{l_2^4}{12}+\frac{31}{24}\pi^2l_2^2+\frac{35\pi^2l_2}{192}-\frac{65\pi^4}{288}-\frac{827\pi^2}{768}+\frac{191}{3072}\Bigg)\\
&+C_A^2C_F^2\Bigg(-\frac{11a_4}{2}-\frac{153\pi^2\zeta_3}{128}-\frac{2779\zeta_3}{384}+\frac{195\zeta_5}{64}-\frac{11l_2^4}{48}-\frac{11}{24}\pi^2l_2^2+\frac{491\pi^2l_2}{192}\\
&+\frac{179\pi^4}{2304}+\frac{1831\pi^2}{2304}-\frac{16873}{165888}\Bigg)+Tn_l\Bigg(C_AC_F^2\Bigg(2a_4-\frac{5\zeta_3}{24}+\frac{l_2^4}{12}+\frac{1}{6}\pi^2l_2^2\\
&-\frac{43\pi^2l_2}{48}-\frac{19\pi^4}{1440}-\frac{385\pi^2}{576}+\frac{62885}{20736}\Bigg)+C_F^3\Bigg(-4a_4-\frac{33\zeta_3}{8}-\frac{l_2^4}{6}-\frac{1}{3}\pi^2l_2^2\\
&+\frac{43\pi^2l_2}{24}+\frac{119\pi^4}{1440}-\frac{97\pi^2}{96}-\frac{1295}{384}\Bigg)\Bigg)+C_F^4\Bigg(18a_4+\frac{3\pi^2\zeta_3}{32}+\frac{459\zeta_3}{64}-\frac{15\zeta_5}{16}\\
&+\frac{3l_2^4}{4}-\frac{3}{4}\pi^2l_2^2-\frac{339\pi^2l_2}{32}+\frac{\pi^4}{32}+\frac{1181\pi^2}{256}+\frac{11135}{2048}\Bigg)
\end{aligned}
$$

$$
\begin{aligned}
&+\left(-\frac{\zeta_3}{3}-\frac{25\pi^2}{144}-\frac{1861}{5184}\right)T^2C_F^2n_hn_l+\left(-\frac{11\zeta_3}{12}-\frac{11\pi^2}{360}+\frac{4943}{10368}\right)T^2C_F^2n_h^2\\
&+\left(\frac{7\zeta_3}{12}+\frac{25\pi^2}{144}-\frac{8665}{10368}\right)T^2C_F^2n_l^2\Bigg)\\
&+l_m^2\Bigg(Tn_h\Bigg(C_AC_F^2\left(-\frac{21\zeta_3}{32}-\frac{5}{16}\pi^2l_2+\frac{65\pi^2}{96}-\frac{751}{144}\right)\\
&+C_F^3\left(\frac{3\zeta_3}{16}+\frac{5\pi^2l_2}{8}-\frac{25\pi^2}{64}-\frac{237}{512}\right)\Bigg)+C_AC_F^3\left(\frac{165\zeta_3}{64}-\frac{55}{32}\pi^2l_2+\frac{275\pi^2}{256}-\frac{8661}{2048}\right)\\
&+C_A^2C_F^2\left(-\frac{165\zeta_3}{128}+\frac{55\pi^2l_2}{64}-\frac{55\pi^2}{192}+\frac{126869}{18432}\right)\\
&+Tn_l\Bigg(C_AC_F^2\left(-\frac{21\zeta_3}{32}-\frac{5}{16}\pi^2l_2-\frac{35\pi^2}{192}-\frac{1519}{576}\right)\\
&+C_F^3\left(\frac{3\zeta_3}{16}+\frac{5\pi^2l_2}{8}-\frac{25\pi^2}{64}-\frac{237}{512}\right)\Bigg)+\left(\frac{623}{576}-\frac{5\pi^2}{48}\right)T^2C_F^2n_hn_l\\
&+\left(\frac{1163}{1152}-\frac{5\pi^2}{24}\right)T^2C_F^2n_h^2+\left(\frac{83}{1152}+\frac{5\pi^2}{48}\right)T^2C_F^2n_l^2+\frac{2169C_F^4}{1024}\Bigg)\\
&+l_m^3\Bigg(Tn_h\left(\frac{45C_F^3}{128}-\frac{1061}{576}C_AC_F^2\right)+Tn_l\left(\frac{45C_F^3}{128}-\frac{1061}{576}C_AC_F^2\right)-\frac{693}{512}C_AC_F^3\\
&+\frac{14101C_A^2C_F^2}{4608}+\frac{67}{144}T^2C_F^2n_hn_l+\frac{67}{288}T^2C_F^2n_h^2+\frac{67}{288}T^2C_F^2n_l^2-\frac{45C_F^4}{256}\Bigg)\\
&+l_m^4\Bigg(-\frac{121}{384}TC_AC_F^2n_h-\frac{121}{384}TC_AC_F^2n_l+\frac{1331C_A^2C_F^2}{3072}+\frac{11}{96}T^2C_F^2n_hn_l\\
&+\frac{11}{192}T^2C_F^2n_h^2+\frac{11}{192}T^2C_F^2n_l^2+\frac{27C_F^4}{1024}\Bigg)\,, \qquad (46)
\end{aligned}
$$

with

$$
l_m=\log\left(\frac{\mu^2}{m^2(\mu)}\right) \qquad (47)
$$

Note that the μ dependence at four-loop order has also been discussed in Ref. [71].

D Counterterm contribution to Z_m^{OS}

In this Appendix we show the four-loop contribution to Z_m^{OS} introduced by the lower loop orders. To be precise we write

$$
Z_m^{\mathrm{OS}}=\sum_{n\geq 0}\left(\frac{\alpha_s(\mu)}{\pi}\right)^n Z_m^{\mathrm{OS},(n)} \qquad (48)
$$

and split $Z_m^{\mathrm{OS},(4)}$ as

$$Z_m^{\mathrm{OS},(4)} = Z_m^{\mathrm{OS},(4)}\Big|_{\mathrm{CT}} + Z_m^{\mathrm{OS},(4)}\Big|_{\text{genuine 4 loop}}, \tag{49}$$

where $Z_m^{\mathrm{OS},(4)}|_{\mathrm{CT}}$ contains all counterterm contributions from the renormalization of the strong coupling constant and quark mass. For $mu^2 = M^2$ it is given by

$$\begin{aligned}
Z_m^{\mathrm{OS},(4)}\Big|_{\mathrm{CT}} = &\Bigg\{T^2 n_h n_l\left(\frac{11C_AC_F}{48}+\frac{17C_F^2}{64}\right)+T^2n_h^2\left(\frac{11C_AC_F}{96}+\frac{11C_F^2}{64}\right)\\
&+Tn_h\left(-\frac{47}{64}C_AC_F^2-\frac{121}{384}C_A^2C_F-\frac{189C_F^3}{256}\right)+T^2n_l^2\left(\frac{11C_AC_F}{96}+\frac{11C_F^2}{96}\right)\\
&+Tn_l\left(-\frac{121}{192}C_AC_F^2-\frac{121}{384}C_A^2C_F-\frac{135C_F^3}{256}\right)\\
&+\frac{1377C_AC_F^3}{1024}+\frac{1331C_A^2C_F^2}{1536}+\frac{1331C_A^3C_F}{4608}-\frac{1}{24}T^3C_Fn_hn_l^2\\
&-\frac{1}{24}T^3C_Fn_h^2n_l-\frac{1}{72}T^3C_Fn_h^3-\frac{1}{72}T^3C_Fn_l^3+\frac{243C_F^4}{256}\Bigg\}\frac{1}{\epsilon^4}\\
&+\Bigg\{T^2n_hn_l\left(\frac{235C_AC_F}{288}+\frac{337C_F^2}{384}\right)+T^2n_h^2\left(\frac{235C_AC_F}{576}+\frac{175C_F^2}{384}\right)\\
&+Tn_h\left(-\frac{1399}{512}C_AC_F^2-\frac{2671C_A^2C_F}{2304}-\frac{559C_F^3}{512}\right)+T^2n_l^2\left(\frac{235C_AC_F}{576}+\frac{27C_F^2}{64}\right)\\
&+Tn_l\left(-\frac{325}{128}C_AC_F^2-\frac{2671C_A^2C_F}{2304}-\frac{5C_F^3}{4}\right)+\frac{1}{256}\left(904-3\pi^2\right)C_AC_F^3\\
&+\frac{3841C_A^2C_F^2}{1024}+\frac{3421C_A^3C_F}{3072}-\frac{7}{48}T^3C_Fn_hn_l^2-\frac{7}{48}T^3C_Fn_h^2n_l\\
&-\frac{7}{144}T^3C_Fn_h^3-\frac{7}{144}T^3C_Fn_l^3-\frac{45C_F^4}{512}\Bigg\}\frac{1}{\epsilon^3}\\
&+\Bigg\{Tn_h\Bigg(C_AC_F^2\left(-\frac{5\zeta_3}{16}+\frac{7\pi^2l_2}{24}+\frac{157\pi^2}{256}-\frac{183953}{9216}\right)\\
&+\left(-\frac{11}{24}\pi^2l_2+\frac{1199\pi^2}{2304}-\frac{59435}{4608}\right)C_A^2C_F\\
&+C_F^3\left(-\frac{21\zeta_3}{16}+\frac{5\pi^2l_2}{4}-\frac{59\pi^2}{256}-\frac{35327}{3072}\right)\Bigg)\\
&+T^2n_h^2\left(C_AC_F\left(\frac{\zeta_3}{8}+\frac{\pi^2l_2}{12}-\frac{181\pi^2}{576}+\frac{7933}{1728}\right)+\left(-\frac{1}{6}\pi^2l_2-\frac{101\pi^2}{384}+\frac{10775}{2304}\right)C_F^2\right)\\
&+T^2n_hn_l\left(C_AC_F\left(\frac{\zeta_3}{4}+\frac{\pi^2l_2}{6}-\frac{49\pi^2}{288}+\frac{6745}{864}\right)+\left(-\frac{1}{3}\pi^2l_2+\frac{\pi^2}{24}+\frac{15769}{2304}\right)C_F^2\right)
\end{aligned}$$

$$
\begin{aligned}
&+C_AC_F^3\left(\frac{1353\zeta_3}{512}-\frac{467}{256}\pi^2l_2+\frac{4149\pi^2}{2048}+\frac{20165}{1536}\right)\\
&+C_A^2C_F^2\left(-\frac{277\zeta_3}{512}+\frac{143\pi^2l_2}{384}+\frac{\pi^4}{1440}+\frac{4103\pi^2}{18432}+\frac{122785}{6144}\right)\\
&+C_A^3C_F\left(-\frac{121\zeta_3}{128}+\frac{121\pi^2l_2}{192}-\frac{4477\pi^2}{27648}+\frac{1953781}{165888}\right)\\
&+Tn_l\left(C_AC_F^2\left(-\frac{35\zeta_3}{64}+\frac{31\pi^2l_2}{96}-\frac{1963\pi^2}{2304}-\frac{10477}{768}\right)\right.\\
&\left.+\left(-\frac{11}{24}\pi^2l_2-\frac{253\pi^2}{2304}-\frac{50723}{4608}\right)C_A^2C_F+C_F^3\left(-\frac{33\zeta_3}{32}+\frac{19\pi^2l_2}{16}-\frac{683\pi^2}{512}-\frac{4391}{768}\right)\right)\\
&+T^2n_l^2\left(C_AC_F\left(\frac{\zeta_3}{8}+\frac{\pi^2l_2}{12}+\frac{83\pi^2}{576}+\frac{5557}{1728}\right)+\left(-\frac{1}{6}\pi^2l_2+\frac{323\pi^2}{1152}+\frac{871}{384}\right)C_F^2\right)\\
&+\left(\frac{11\pi^2}{144}-\frac{1193}{864}\right)T^3C_Fn_h^2n_l+\left(-\frac{977}{864}-\frac{\pi^2}{144}\right)T^3C_Fn_hn_l^2\\
&+\left(\frac{23\pi^2}{432}-\frac{1409}{2592}\right)T^3C_Fn_h^3+C_F^4\left(\frac{1107\zeta_3}{256}-\frac{369}{128}\pi^2l_2+\frac{297\pi^2}{128}+\frac{2787}{1024}\right)\\
&\left.+\left(-\frac{761}{2592}-\frac{13\pi^2}{432}\right)T^3C_Fn_l^3\right\}\frac{1}{\epsilon^2}\\
&+\left\{\left(\frac{625l_2^4}{128}+\frac{225}{64}\pi^2l_2^2-\frac{745\pi^2l_2}{16}+\frac{1875a_4}{16}+\frac{3\pi^2\zeta_3}{64}+\frac{4695\zeta_3}{64}-\frac{75\zeta_5}{64}-\frac{2311\pi^4}{2560}\right.\right.\\
&\left.+\frac{65941\pi^2}{3072}+\frac{44617}{2048}\right)C_F^4+C_A\left(\frac{2557l_2^4}{768}+\frac{2341}{384}\pi^2l_2^2-\frac{1775\pi^2l_2}{64}+\frac{2557a_4}{32}\right.\\
&\left.+\frac{317\pi^2\zeta_3}{64}+\frac{39451\zeta_3}{512}-\frac{475\zeta_5}{32}-\frac{56531\pi^4}{46080}+\frac{169661\pi^2}{12288}+\frac{169787}{3072}\right)C_F^3\\
&+C_A^2\left(-\frac{113l_2^4}{144}+\frac{79}{288}\pi^2l_2^2+\frac{10145\pi^2l_2}{1152}-\frac{113a_4}{6}+\frac{115\pi^2\zeta_3}{768}-\frac{2123\zeta_3}{4608}\right.\\
&\left.+\frac{187\zeta_5}{128}-\frac{5039\pi^4}{92160}+\frac{27593\pi^2}{12288}+\frac{3298805}{36864}\right)C_F^2\\
&+n_l^3T^3\left(-\frac{77\zeta_3}{108}-\frac{611\pi^2}{2592}-\frac{22697}{15552}\right)C_F\\
&+n_hn_l^2T^3\left(-\frac{1}{3}\pi^2l_2+\frac{13\zeta_3}{36}+\frac{25\pi^2}{864}-\frac{32417}{5184}\right)C_F\\
&+n_h^3T^3\left(-\frac{1}{3}\pi^2l_2+\frac{193\zeta_3}{108}+\frac{3749\pi^2}{12960}-\frac{51857}{15552}\right)C_F\\
&+n_h^2n_lT^3\left(-\frac{2}{3}\pi^2l_2+\frac{103\zeta_3}{36}+\frac{2393\pi^2}{4320}-\frac{42137}{5184}\right)C_F
\end{aligned}
$$

$$
\begin{aligned}
&+C_A^3\bigg(-\frac{605l_2^4}{576}-\frac{605}{288}\pi^2l_2^2+\frac{2405\pi^2l_2}{288}-\frac{605a_4}{24}-\frac{561\pi^2\zeta_3}{256}-\frac{148433\zeta_3}{6912}+\frac{715\zeta_5}{128}\\
&+\frac{25091\pi^4}{69120}+\frac{169519\pi^2}{165888}+\frac{64234201}{995328}\bigg)C_F+n_l^2T^2\bigg(\bigg(\frac{5l_2^4}{18}+\frac{5}{9}\pi^2l_2^2-\frac{20\pi^2l_2}{9}\\
&+\frac{20a_4}{3}+\frac{2257\zeta_3}{288}-\frac{49\pi^4}{432}+\frac{5509\pi^2}{2304}+\frac{77327}{6912}\bigg)C_F^2\\
&+C_A\bigg(-\frac{5l_2^4}{36}-\frac{5}{18}\pi^2l_2^2+\frac{10\pi^2l_2}{9}-\frac{10a_4}{3}+\frac{85\zeta_3}{36}+\frac{41\pi^4}{1080}+\frac{4655\pi^2}{3456}+\frac{343919}{20736}\bigg)C_F\bigg)\\
&+n_h^2T^2\bigg(\bigg(\frac{5l_2^4}{18}+\frac{2}{9}\pi^2l_2^2+\frac{43\pi^2l_2}{18}+\frac{20a_4}{3}-\frac{369\zeta_3}{32}-\frac{7\pi^4}{432}-\frac{79751\pi^2}{34560}+\frac{109217}{4608}\bigg)C_F^2\\
&+C_A\bigg(-\frac{5l_2^4}{36}-\frac{1}{9}\pi^2l_2^2+\frac{53\pi^2l_2}{9}-\frac{10a_4}{3}+\frac{\pi^2\zeta_3}{8}-\frac{721\zeta_3}{72}-\frac{5\zeta_5}{8}-\frac{23\pi^4}{2160}\\
&-\frac{27391\pi^2}{5760}+\frac{610895}{20736}\bigg)C_F\bigg)\\
&+n_hn_lT^2\bigg(\bigg(\frac{5l_2^4}{9}+\frac{7}{9}\pi^2l_2^2+\frac{\pi^2l_2}{24}+\frac{40a_4}{3}-\frac{79\zeta_3}{48}-\frac{7\pi^4}{54}-\frac{143\pi^2}{216}+\frac{475145}{13824}\bigg)C_F^2\\
&+C_A\bigg(-\frac{5l_2^4}{18}-\frac{7}{18}\pi^2l_2^2+7\pi^2l_2-\frac{20a_4}{3}+\frac{\pi^2\zeta_3}{8}-\frac{551\zeta_3}{72}-\frac{5\zeta_5}{8}+\frac{59\pi^4}{2160}\\
&-\frac{6893\pi^2}{1728}+\frac{477407}{10368}\bigg)C_F\bigg)\\
&+n_lT\bigg(\bigg(-\frac{101l_2^4}{48}-\frac{65}{24}\pi^2l_2^2+\frac{155\pi^2l_2}{8}-\frac{101a_4}{2}-\frac{\pi^2\zeta_3}{16}-\frac{5045\zeta_3}{128}+\frac{5\zeta_5}{8}\\
&+\frac{1723\pi^4}{2880}-\frac{11719\pi^2}{1024}-\frac{15091}{512}\bigg)C_F^3+C_A\bigg(-\frac{137l_2^4}{288}-\frac{245}{144}\pi^2l_2^2+\frac{371\pi^2l_2}{144}\\
&-\frac{137a_4}{12}-\frac{19\pi^2\zeta_3}{16}-\frac{1831\zeta_3}{72}+\frac{45\zeta_5}{16}+\frac{6601\pi^4}{17280}-\frac{15377\pi^2}{2304}-\frac{438589}{6912}\bigg)C_F^2\\
&+C_A^2\bigg(\frac{55l_2^4}{72}+\frac{55}{36}\pi^2l_2^2-\frac{883\pi^2l_2}{144}+\frac{55a_4}{3}+\frac{51\pi^2\zeta_3}{64}+\frac{1949\zeta_3}{288}-\frac{65\zeta_5}{32}\\
&-\frac{817\pi^4}{3456}-\frac{10337\pi^2}{4608}-\frac{1610957}{27648}\bigg)C_F\bigg)+n_hT\bigg(\bigg(-\frac{19l_2^4}{8}-\frac{11}{8}\pi^2l_2^2\\
&+\frac{4679\pi^2l_2}{768}-57a_4-\frac{\pi^2\zeta_3}{16}-\frac{5777\zeta_3}{1536}+\frac{5\zeta_5}{8}+\frac{139\pi^4}{480}-\frac{13829\pi^2}{27648}\\
&-\frac{819703}{18432}\bigg)C_F^3+C_A\bigg(-\frac{5l_2^4}{18}-\frac{109}{72}\pi^2l_2^2-\frac{711\pi^2l_2}{32}-\frac{20a_4}{3}-\frac{105\pi^2\zeta_3}{64}\\
&+\frac{16697\zeta_3}{768}+\frac{315\zeta_5}{64}+\frac{2261\pi^4}{8640}+\frac{83269\pi^2}{4608}-\frac{5891549}{55296}\bigg)C_F^2\\
&+C_A^2\bigg(\frac{55l_2^4}{72}+\frac{77}{72}\pi^2l_2^2-\frac{67\pi^2l_2}{4}+\frac{55a_4}{3}+\frac{29\pi^2\zeta_3}{64}+\frac{6305\zeta_3}{288}-\frac{5\zeta_5}{16}
\end{aligned}
$$

$$
\begin{aligned}
&- \frac{355\pi^4}{3456} + \frac{144577\pi^2}{13824} - \frac{2188757}{27648}\Big) C_F \Big) \Big\} \frac{1}{\epsilon} \\
&+ \Big\{ \Big(- \frac{5497 l_2^5}{960} - \frac{25}{32}\pi^2 l_2^4 + \frac{1113 l_2^4}{16} - \frac{1753}{288}\pi^2 l_2^3 + \frac{49}{32}\pi^4 l_2^2 + \frac{3193}{24}\pi^2 l_2^2 \\
&- \frac{597}{32}\pi^2 \zeta_3 l_2 + \frac{47879\pi^4 l_2}{11520} - \frac{580283\pi^2 l_2}{1536} + \frac{273\zeta_3^2}{128} + \frac{3339 a_4}{2} + \frac{5497 a_5}{8} \\
&- \frac{30763\pi^2\zeta_3}{768} + \frac{702863\zeta_3}{1024} - \frac{263441\zeta_5}{512} + \frac{1349\pi^6}{7560} - \frac{50003\pi^4}{11520} - \frac{75 a_4 \pi^2}{4} \\
&+ \frac{954883\pi^2}{9216} + \frac{1233161}{12288}\Big) C_F^4 \\
&+ C_A \Big(- \frac{11719 l_2^5}{1920} - \frac{41}{32}\pi^2 l_2^4 + \frac{7675 l_2^4}{192} - \frac{11503}{576}\pi^2 l_2^3 + \frac{17}{32}\pi^4 l_2^2 + \frac{15679}{96}\pi^2 l_2^2 \\
&- \frac{789}{32}\pi^2\zeta_3 l_2 + \frac{66053\pi^4 l_2}{23040} - \frac{168439\pi^2 l_2}{1024} + \frac{3937\zeta_3^2}{64} + \frac{7675 a_4}{8} + \frac{11719 a_5}{16} \\
&+ \frac{1529\pi^2\zeta_3}{384} + \frac{2917189\zeta_3}{6144} - \frac{895973\zeta_5}{1024} + \frac{4763\pi^6}{10080} - \frac{10254293\pi^4}{737280} - \frac{123 a_4\pi^2}{4} \\
&+ \frac{7263359\pi^2}{73728} + \frac{518789}{2048}\Big) C_F^3 \\
&+ C_A^2 \Big(\frac{89 l_2^5}{144} - \frac{97}{384}\pi^2 l_2^4 - \frac{43913 l_2^4}{3456} - \frac{595}{432}\pi^2 l_2^3 + \frac{169}{384}\pi^4 l_2^2 - \frac{11153\pi^2 l_2^2}{1728} \\
&- \frac{751}{128}\pi^2\zeta_3 l_2 - \frac{11185\pi^4 l_2}{6912} + \frac{169367\pi^2 l_2}{1728} + \frac{4813\zeta_3^2}{512} - \frac{43913 a_4}{144} - \frac{445 a_5}{6} \\
&+ \frac{179791\pi^2\zeta_3}{9216} - \frac{12445\zeta_3}{9216} - \frac{24275\zeta_5}{1024} + \frac{19679\pi^6}{241920} - \frac{17671879\pi^4}{6635520} - \frac{97 a_4\pi^2}{16} \\
&+ \frac{5799935\pi^2}{221184} + \frac{92980613}{221184}\Big) C_F^2 \\
&+ n_l^3 T^3 \Big(- \frac{3073\zeta_3}{648} - \frac{259\pi^4}{2160} - \frac{6035\pi^2}{5184} - \frac{620897}{93312}\Big) C_F \\
&+ n_h n_l^2 T^3 \Big(\frac{5 l_2^4}{9} + \frac{10}{9}\pi^2 l_2^2 - \frac{31\pi^2 l_2}{9} + \frac{40 a_4}{3} + \frac{1319\zeta_3}{216} - \frac{289\pi^4}{2160} \\
&+ \frac{11\pi^2}{576} - \frac{974489}{31104}\Big) C_F + n_h^3 T^3 \Big(\frac{5 l_2^4}{9} + \frac{4}{9}\pi^2 l_2^2 - \frac{83\pi^2 l_2}{45} + \frac{40 a_4}{3} \\
&+ \frac{34099\zeta_3}{3240} - \frac{167\pi^4}{2160} + \frac{220129\pi^2}{129600} - \frac{8242477}{466560}\Big) C_F \\
&+ n_h^2 n_l T^3 \Big(\frac{10 l_2^4}{9} + \frac{14}{9}\pi^2 l_2^2 - \frac{238\pi^2 l_2}{45} + \frac{80 a_4}{3} + \frac{23083\zeta_3}{1080} - \frac{197\pi^4}{2160} \\
&+ \frac{124493\pi^2}{43200} - \frac{6585109}{155520}\Big) C_F + C_A^3 \Big(\frac{2783 l_2^5}{1440} + \frac{209}{384}\pi^2 l_2^4 - \frac{5329 l_2^4}{432}
\end{aligned}
$$

$$
\begin{aligned}
&+\frac{2783}{432}\pi^2 l_2^3-\frac{209}{384}\pi^4 l_2^2-\frac{23429}{432}\pi^2 l_2^2+\frac{1463}{128}\pi^2\zeta_3 l_2-\frac{7381\pi^4 l_2}{17280}\\
&+\frac{67979\pi^2 l_2}{1728}-\frac{1507\zeta_3^2}{64}-\frac{5329a_4}{18}-\frac{2783a_5}{12}-\frac{187\pi^2\zeta_3}{256}-\frac{3503635\zeta_3}{41472}\\
&+\frac{203005\zeta_5}{768}-\frac{104159\pi^6}{483840}+\frac{219365\pi^4}{41472}+\frac{209a_4\pi^2}{16}+\frac{1818263\pi^2}{331776}+\frac{1829511217}{5971968}\Bigg)C_F\\
&+n_h^2T^2\Bigg(\Bigg(-\frac{l_2^5}{3}-\frac{443l_2^4}{108}-\frac{4}{9}\pi^2 l_2^3-\frac{907}{108}\pi^2 l_2^2+\frac{11\pi^4 l_2}{36}+\frac{16829\pi^2 l_2}{540}-\frac{886a_4}{9}\\
&+40a_5-\frac{233\pi^2\zeta_3}{48}-\frac{1643\zeta_3}{20}-\frac{385\zeta_5}{24}+\frac{317377\pi^4}{414720}-\frac{730669\pi^2}{38400}+\frac{52140391}{414720}\Bigg)C_F^2\\
&+C_A\Bigg(\frac{l_2^5}{6}+\frac{1}{8}\pi^2 l_2^4-\frac{233l_2^4}{27}+\frac{2}{9}\pi^2 l_2^3-\frac{1}{8}\pi^4 l_2^2-\frac{1613}{54}\pi^2 l_2^2+\frac{21}{8}\pi^2\zeta_3 l_2\\
&-\frac{11\pi^4 l_2}{72}+\frac{27899\pi^2 l_2}{540}+\frac{19\zeta_3^2}{8}-\frac{1864a_4}{9}-20a_5+\frac{175\pi^2\zeta_3}{48}-\frac{665293\zeta_3}{4320}\\
&+\frac{37\zeta_5}{48}-\frac{41\pi^6}{1080}+\frac{3851\pi^4}{3240}+3a_4\pi^2-\frac{18335563\pi^2}{1036800}+\frac{31646753}{207360}\Bigg)C_F\Bigg)\\
&+n_l^2T^2\Bigg(\Bigg(-\frac{23l_2^5}{45}+\frac{89l_2^4}{27}-\frac{46}{27}\pi^2 l_2^3+\frac{178}{27}\pi^2 l_2^2+\frac{61\pi^4 l_2}{540}-\frac{355\pi^2 l_2}{27}\\
&+\frac{712a_4}{9}+\frac{184a_5}{3}-\frac{95\pi^2\zeta_3}{48}+\frac{32747\zeta_3}{576}-\frac{1657\zeta_5}{24}-\frac{78943\pi^4}{414720}\\
&+\frac{191657\pi^2}{13824}+\frac{735901}{13824}\Bigg)C_F^2+C_A\Bigg(\frac{23l_2^5}{90}-\frac{89l_2^4}{54}+\frac{23}{27}\pi^2 l_2^3-\frac{89}{27}\pi^2 l_2^2\\
&-\frac{61\pi^4 l_2}{1080}+\frac{355\pi^2 l_2}{54}-\frac{356a_4}{9}-\frac{92a_5}{3}+\frac{37\pi^2\zeta_3}{48}+\frac{14887\zeta_3}{864}+\frac{1519\zeta_5}{48}\\
&+\frac{325\pi^4}{324}+\frac{298109\pi^2}{41472}+\frac{3159661}{41472}\Bigg)C_F\Bigg)\\
&+n_h n_l T^2\Bigg(\Bigg(-\frac{38l_2^5}{45}-\frac{31l_2^4}{72}-\frac{58}{27}\pi^2 l_2^3-\frac{155}{36}\pi^2 l_2^2+\frac{113\pi^4 l_2}{270}+\frac{191\pi^2 l_2}{8}\\
&-\frac{31a_4}{3}+\frac{304a_5}{3}-\frac{41\pi^2\zeta_3}{6}-\frac{5293\zeta_3}{144}-\frac{1021\zeta_5}{12}-\frac{20837\pi^4}{69120}-\frac{5063\pi^2}{864}+\frac{14881105}{82944}\Bigg)C_F^2\\
&+C_A\Bigg(\frac{19l_2^5}{45}+\frac{1}{8}\pi^2 l_2^4-\frac{185l_2^4}{18}+\frac{29}{27}\pi^2 l_2^3-\frac{1}{8}\pi^4 l_2^2-35\pi^2 l_2^2+\frac{21}{8}\pi^2\zeta_3 l_2-\frac{113\pi^4 l_2}{540}\\
&+\frac{2255\pi^2 l_2}{36}+\frac{19\zeta_3^2}{8}-\frac{740a_4}{3}-\frac{152a_5}{3}+\frac{53\pi^2\zeta_3}{12}-\frac{65105\zeta_3}{432}+\frac{389\zeta_5}{12}-\frac{41\pi^6}{1080}\\
&+\frac{27\pi^4}{16}+3a_4\pi^2-\frac{254659\pi^2}{20736}+\frac{4764781}{20736}\Bigg)C_F\Bigg)\\
&+n_hT\Bigg(\Bigg(\frac{57l_2^5}{20}+\frac{1}{8}\pi^2 l_2^4-\frac{2641l_2^4}{256}+\frac{11}{4}\pi^2 l_2^3-\frac{1}{8}\pi^4 l_2^2-\frac{187}{128}\pi^2 l_2^2+\frac{21}{8}\pi^2\zeta_3 l_2
\end{aligned}
$$

$$
\begin{aligned}
&-\frac{521\pi^4 l_2}{160}+\frac{823\pi^2 l_2}{256}-\frac{\zeta_3^2}{2}-\frac{7923a_4}{32}-342a_5+\frac{5743\pi^2\zeta_3}{192}-\frac{107213\zeta_3}{4608}\\
&+\frac{6503\zeta_5}{32}-\frac{5\pi^6}{189}+\frac{63667\pi^4}{184320}+3a_4\pi^2+\frac{2023643\pi^2}{165888}-\frac{26730911}{110592}\bigg)C_F^3\\
&+C_A\bigg(\frac{37l_2^5}{45}-\frac{19}{96}\pi^2 l_2^4+\frac{12683l_2^4}{384}+\frac{503}{108}\pi^2 l_2^3+\frac{19}{96}\pi^4 l_2^2+\frac{127015\pi^2 l_2^2}{1152}-\frac{133}{32}\pi^2\zeta_3 l_2\\
&+\frac{5041\pi^4 l_2}{8640}-\frac{18911\pi^2 l_2}{72}-\frac{3219\zeta_3^2}{128}+\frac{12683a_4}{16}-\frac{296a_5}{3}-\frac{2437\pi^2\zeta_3}{256}+\frac{284675\zeta_3}{512}\\
&+\frac{134183\zeta_5}{768}+\frac{7\pi^6}{216}-\frac{103817\pi^4}{55296}-\frac{19a_4\pi^2}{4}+\frac{5872135\pi^2}{82944}-\frac{183814805}{331776}\bigg)C_F^2\\
&+C_A^2\bigg(-\frac{209l_2^5}{180}-\frac{13}{24}\pi^2 l_2^4+\frac{433l_2^4}{18}-\frac{319}{108}\pi^2 l_2^3+\frac{13}{24}\pi^4 l_2^2+\frac{1183}{12}\pi^2 l_2^2-\frac{91}{8}\pi^2\zeta_3 l_2\\
&+\frac{1243\pi^4 l_2}{2160}-\frac{10241\pi^2 l_2}{72}+\frac{65\zeta_3^2}{32}+\frac{1732a_4}{3}+\frac{418a_5}{3}-\frac{937\pi^2\zeta_3}{96}+\frac{430415\zeta_3}{1152}\\
&-\frac{9431\zeta_5}{96}+\frac{22097\pi^6}{120960}-\frac{53237\pi^4}{11520}-13a_4\pi^2+\frac{347143\pi^2}{10368}-\frac{197507311}{497664}\bigg)C_F\bigg)\\
&+n_l T\bigg(\bigg(\frac{383l_2^5}{120}+\frac{1}{8}\pi^2 l_2^4-\frac{685l_2^4}{24}+\frac{275}{36}\pi^2 l_2^3-\frac{1}{8}\pi^4 l_2^2-\frac{166}{3}\pi^2 l_2^2+\frac{21}{8}\pi^2\zeta_3 l_2\\
&-\frac{257\pi^4 l_2}{180}+\frac{579\pi^2 l_2}{4}-\frac{\zeta_3^2}{2}-685a_4-383a_5+\frac{3169\pi^2\zeta_3}{192}-\frac{245419\zeta_3}{768}+\frac{23615\zeta_5}{64}\\
&-\frac{5\pi^6}{189}+\frac{484063\pi^4}{184320}+3a_4\pi^2-\frac{1185613\pi^2}{18432}-\frac{152405}{1024}\bigg)C_F^3\\
&+C_A\bigg(\frac{175l_2^5}{144}+\frac{1}{3}\pi^2 l_2^4-\frac{1661l_2^4}{432}+\frac{1199}{216}\pi^2 l_2^3-\frac{1}{3}\pi^4 l_2^2-\frac{3247}{108}\pi^2 l_2^2+7\pi^2\zeta_3 l_2\\
&+\frac{5\pi^4 l_2}{54}-\frac{385\pi^2 l_2}{54}-\frac{249\zeta_3^2}{16}-\frac{1661a_4}{18}-\frac{875a_5}{6}-\frac{1763\pi^2\zeta_3}{384}-\frac{87917\zeta_3}{576}+\frac{85783\zeta_5}{384}\\
&-\frac{7709\pi^6}{60480}+\frac{2344277\pi^4}{829440}+8a_4\pi^2-\frac{643145\pi^2}{13824}-\frac{151453}{512}\bigg)C_F^2\\
&+C_A^2\bigg(-\frac{253l_2^5}{180}-\frac{19}{96}\pi^2 l_2^4+\frac{3913l_2^4}{432}-\frac{253}{54}\pi^2 l_2^3+\frac{19}{96}\pi^4 l_2^2+\frac{6235}{216}\pi^2 l_2^2-\frac{133}{32}\pi^2\zeta_3 l_2\\
&+\frac{671\pi^4 l_2}{2160}-\frac{14093\pi^2 l_2}{432}+\frac{137\zeta_3^2}{16}+\frac{3913a_4}{18}+\frac{506a_5}{3}-\frac{89\pi^2\zeta_3}{48}+\frac{23219\zeta_3}{1152}-\frac{8791\zeta_5}{48}\\
&+\frac{9469\pi^6}{120960}-\frac{392849\pi^4}{103680}-\frac{19a_4\pi^2}{4}-\frac{264949\pi^2}{20736}-\frac{134979991}{497664}\bigg)C_F\bigg)\bigg\}\\
&+\xi\Bigg[\bigg\{Tn_h\bigg(\frac{1}{256}C_A {C_F}^2-\frac{9{C_F}^3}{128}\bigg)+\frac{477C_A{C_F}^3}{2048}-\frac{9}{128}T{C_F}^3 n_l+\frac{297{C_F}^4}{512}\bigg\}\frac{1}{\epsilon^4}\\
&+\bigg\{Tn_h\bigg(-\frac{5}{768}C_A{C_F}^2-\frac{75{C_F}^3}{256}\bigg)+\bigg(\frac{2271}{2048}-\frac{3\pi^2}{512}\bigg)C_A{C_F}^3
\end{aligned}
$$

$$
\begin{aligned}
&-\frac{75}{256}TC_F{}^3n_l+\frac{999C_F{}^4}{1024}\bigg\}\frac{1}{\epsilon^3}\\
&+\bigg\{\bigg(\frac{9\zeta_3}{1024}-\frac{\pi^4}{5760}+\frac{1}{1024}\bigg)C_A{}^2C_F{}^2+Tn_h\bigg(\bigg(\frac{31}{768}+\frac{\pi^2}{768}\bigg)C_AC_F{}^2\\
&+\bigg(\frac{9\pi^2}{128}-\frac{913}{512}\bigg)C_F{}^3\bigg)+C_AC_F{}^3\bigg(-\frac{9\zeta_3}{32}+\frac{9\pi^2l_2}{64}+\frac{37\pi^2}{2048}+\frac{1387}{256}\bigg)\\
&+C_F{}^4\bigg(\frac{27\zeta_3}{64}-\frac{9}{32}\pi^2l_2+\frac{225\pi^2}{512}+\frac{12069}{2048}\bigg)+\bigg(-\frac{697}{512}-\frac{9\pi^2}{128}\bigg)TC_F{}^3n_l\bigg\}\frac{1}{\epsilon^2}\\
&+\bigg\{C_AC_F{}^3\bigg(-\frac{27a_4}{8}-\frac{1245\zeta_3}{512}-\frac{9l_2{}^4}{64}-\frac{9}{32}\pi^2l_2{}^2+\frac{15\pi^2l_2}{16}+\frac{21\pi^4}{512}+\frac{377\pi^2}{6144}\\
&+\frac{80197}{4096}\bigg)+C_F{}^4\bigg(\frac{27a_4}{4}+\frac{639\zeta_3}{128}+\frac{9l_2{}^4}{32}+\frac{9}{16}\pi^2l_2{}^2-\frac{15\pi^2l_2}{8}-\frac{63\pi^4}{640}\\
&+\frac{1659\pi^2}{1024}+\frac{49519}{4096}\bigg)+\bigg(-\frac{1}{192}\pi^2\zeta_3+\frac{51\zeta_3}{1024}-\frac{7\zeta_5}{512}-\frac{383\pi^4}{552960}+\frac{3\pi^2}{1024}+\frac{43}{3072}\bigg)C_A{}^2C_F{}^2\\
&+Tn_h\bigg(\bigg(\frac{5\zeta_3}{192}-\frac{5\pi^2}{2304}-\frac{97}{768}\bigg)C_AC_F{}^2+C_F{}^3\bigg(\frac{33\zeta_3}{16}-\frac{9}{16}\pi^2l_2+\frac{111\pi^2}{256}-\frac{6899}{1024}\bigg)\bigg)\\
&+\bigg(-\frac{15\zeta_3}{32}-\frac{75\pi^2}{256}-\frac{4955}{1024}\bigg)TC_F{}^3n_l\bigg\}\frac{1}{\epsilon}\\
&+Tn_h\bigg(C_F{}^3\bigg(\frac{27a_4}{2}+\frac{739\zeta_3}{64}+\frac{9l_2{}^4}{16}+\frac{9}{8}\pi^2l_2{}^2-\frac{51\pi^2l_2}{16}-\frac{9\pi^4}{128}+\frac{997\pi^2}{512}-\frac{54873}{2048}\bigg)\\
&+\bigg(-\frac{25\zeta_3}{576}-\frac{\pi^4}{768}+\frac{31\pi^2}{2304}+\frac{1309}{2304}\bigg)C_AC_F{}^2\bigg)+C_AC_F{}^3\bigg(-\frac{45a_4}{2}-\frac{81a_5}{4}+\frac{37\pi^2\zeta_3}{128}\\
&-\frac{6083\zeta_3}{512}+\frac{5157\zeta_5}{256}+\frac{27l_2{}^5}{160}-\frac{15l_2{}^4}{16}+\frac{9}{16}\pi^2l_2{}^3-\frac{15}{8}\pi^2l_2{}^2-\frac{63\pi^4l_2}{640}+\frac{143\pi^2l_2}{32}\\
&+\frac{533\pi^4}{2048}+\frac{2297\pi^2}{3072}+\frac{609965}{8192}\bigg)+C_F{}^4\bigg(45a_4+\frac{81a_5}{2}-\frac{45\pi^2\zeta_3}{64}+\frac{7077\zeta_3}{256}-\frac{5481\zeta_5}{128}\\
&-\frac{27l_2{}^5}{80}+\frac{15l_2{}^4}{8}-\frac{9}{8}\pi^2l_2{}^3+\frac{15}{4}\pi^2l_2{}^2+\frac{63\pi^4l_2}{320}-\frac{143\pi^2l_2}{16}-\frac{699\pi^4}{2560}+\frac{17449\pi^2}{2048}+\frac{433933}{8192}\bigg)\\
&+\bigg(-\frac{25\zeta_3{}^2}{512}-\frac{115\pi^2\zeta_3}{9216}+\frac{265\zeta_3}{1024}+\frac{391\zeta_5}{3072}-\frac{5\pi^6}{6912}-\frac{349\pi^4}{110592}+\frac{91\pi^2}{3072}+\frac{125}{1024}\bigg)C_A{}^2C_F{}^2\\
&+\bigg(-\frac{125\zeta_3}{64}-\frac{9\pi^4}{128}-\frac{697\pi^2}{512}-\frac{35505}{2048}\bigg)TC_F{}^3n_l\bigg]\\
&+\xi^2\bigg[\bigg\{\frac{27C_F{}^4}{1024}-\frac{27C_AC_F{}^3}{2048}\bigg\}\frac{1}{\epsilon^4}\\
&+\bigg\{\frac{27C_F{}^4}{512}-\frac{135C_AC_F{}^3}{4096}\bigg\}\frac{1}{\epsilon^3}
\end{aligned}
$$

$$
\begin{aligned}
&+\left\{\left(-\frac{1071}{4096}-\frac{27\pi^2}{2048}\right)C_A{C_F}^3+\left(\frac{117}{256}+\frac{27\pi^2}{1024}\right){C_F}^4\right\}\frac{1}{\epsilon^2}\\
&+\left\{\left(-\frac{45\zeta_3}{512}-\frac{135\pi^2}{4096}-\frac{2117}{4096}\right)C_A{C_F}^3+\left(\frac{45\zeta_3}{256}+\frac{27\pi^2}{512}+\frac{169}{256}\right){C_F}^4\right\}\frac{1}{\epsilon}\\
&+\left(-\frac{225\zeta_3}{1024}-\frac{27\pi^4}{2048}-\frac{1071\pi^2}{4096}-\frac{14895}{4096}\right)C_A{C_F}^3\\
&+\left(\frac{45\zeta_3}{128}+\frac{27\pi^4}{1024}+\frac{117\pi^2}{256}+\frac{1531}{256}\right){C_F}^4\Bigg],
\end{aligned}
\tag{50}
$$

where a_n and l_2 are given in Eqs. (39) and (44), respectively. The QCD gauge parapeter ξ is defined via the gluon propagator

$$
D_g^{\mu\nu}(q) \;=\; -i\,\frac{g^{\mu\nu}-\xi\frac{q^\mu q^\nu}{q^2}}{q^2+i\varepsilon}\,. \tag{51}
$$

E Analytic results for z_m

In this Appendix we repeat for convenience the coefficients of the colour structures presented in Subsection 3.3 which are known analytically [62].

$$
\begin{aligned}
Z_m^{FLLL} &= \frac{317\zeta_3}{432}+\frac{71\pi^4}{4320}+\frac{89\pi^2}{648}+\frac{42979}{186624}\,,\\
Z_m^{FLLH} &= \frac{5\zeta_3}{144}-\frac{19\pi^4}{480}+\frac{\pi^2}{6}+\frac{128515}{62208}\,,\\
Z_m^{FFLL} &= \frac{2l_2^5}{45}-\frac{11l_2^4}{27}+\frac{4}{27}\pi^2l_2^3-\frac{22}{27}\pi^2l_2^2+\frac{31}{540}\pi^4l_2+\frac{103}{54}\pi^2l_2\\
&\quad-\frac{88a_4}{9}-\frac{16a_5}{3}+\frac{305\zeta_5}{48}+\frac{3\pi^2\zeta_3}{8}-\frac{2839\zeta_3}{576}+\frac{3683\pi^4}{51840}-\frac{5309\pi^2}{3456}-\frac{2396921}{497664}\,,\\
Z_m^{FALL} &= -\frac{1}{45}l_2^5+\frac{11l_2^4}{54}-\frac{2}{27}\pi^2l_2^3+\frac{11}{27}\pi^2l_2^2-\frac{31\pi^4l_2}{1080}-\frac{103}{108}\pi^2l_2+\frac{44a_4}{9}\\
&\quad+\frac{8a_5}{3}-\frac{41\zeta_5}{24}-\frac{13\pi^2\zeta_3}{48}-\frac{3245\zeta_3}{576}-\frac{4723\pi^4}{51840}-\frac{527\pi^2}{384}-\frac{2708353}{497664}\,,
\end{aligned}
\tag{52}
$$

where a_n and l_2 are given in Eqs. (39) and (44), respectively.

F $Z_m^{\overline{\rm MS}}$ for general SU(N_c) gauge group

In this Appendix we present results for the $\overline{\rm MS}$ renormalization constant $Z_m^{\overline{\rm MS}}$ up to four-loop order [22,23] expressed in terms of SU(N_c) colour factors. It has been obtained from the quark mass anomalous dimension given in [23].

$$
Z_m^{\overline{\rm MS}} = 1-\frac{3C_F}{4\epsilon}\frac{\alpha_s}{\pi}
$$

$$
\begin{aligned}
&+\left\{\left[\frac{9C_F^2}{32}+\frac{11C_AC_F}{32}-\frac{1}{8}n_fTC_F\right]\frac{1}{\epsilon^2}+\left[-\frac{3C_F^2}{64}-\frac{97C_AC_F}{192}+\frac{5}{48}n_fTC_F\right]\frac{1}{\epsilon}\right\}\left(\frac{\alpha_s}{\pi}\right)^2\\
&+\left\{\left[-\frac{9C_F^3}{128}-\frac{33}{128}C_AC_F^2-\frac{121}{576}C_A^2C_F-\frac{1}{36}n_f^2T^2C_F+\left(\frac{3C_F^2}{32}+\frac{11C_AC_F}{72}\right)n_fT\right]\frac{1}{\epsilon^3}\right.\\
&\quad+\left[\frac{9C_F^3}{256}+\frac{313}{768}C_AC_F^2+\frac{1679C_A^2C_F}{3456}+\frac{5}{216}n_f^2T^2C_F+\left(-\frac{29C_F^2}{192}-\frac{121C_AC_F}{432}\right)n_fT\right]\frac{1}{\epsilon^2}\\
&\quad+\left[-\frac{43C_F^3}{128}+\frac{43}{256}C_AC_F^2-\frac{11413C_A^2C_F}{20736}+\frac{35n_f^2T^2C_F}{1296}\right.\\
&\qquad\left.\left.+n_fT\left(\left(\frac{23}{96}-\frac{\zeta_3}{4}\right)C_F^2+C_A\left(\frac{\zeta_3}{4}+\frac{139}{1296}\right)C_F\right)\right]\frac{1}{\epsilon}\right\}\left(\frac{\alpha_s}{\pi}\right)^3\\
&+\left\{\left[\frac{27C_F^4}{2048}+\frac{99C_AC_F^3}{1024}+\frac{1331C_A^2C_F^2}{6144}+\frac{1331C_A^3C_F}{9216}-\frac{1}{144}n_f^3T^3C_F\right.\right.\\
&\qquad\left.+\left(\frac{11C_F^2}{384}+\frac{11C_AC_F}{192}\right)n_f^2T^2+\left(-\frac{9C_F^3}{256}-\frac{121}{768}C_AC_F^2-\frac{121}{768}C_A^2C_F\right)n_fT\right]\frac{1}{\epsilon^4}\\
&\quad+\left[-\frac{27C_F^4}{2048}-\frac{23}{128}C_AC_F^3-\frac{1285C_A^2C_F^2}{2304}-\frac{25201C_A^3C_F}{55296}+\frac{5}{864}n_f^3T^3C_F\right.\\
&\qquad\left.+\left(-\frac{37C_F^2}{576}-\frac{43C_AC_F}{384}\right)n_f^2T^2+\left(\frac{23C_F^3}{256}+\frac{943C_AC_F^2}{2304}+\frac{1981C_A^2C_F}{4608}\right)n_fT\right]\frac{1}{\epsilon^3}\\
&\quad+\left[\frac{2073C_F^4}{8192}+\frac{527C_AC_F^3}{4096}+\frac{97661C_A^2C_F^2}{221184}+\frac{236333C_A^3C_F}{331776}+\frac{35n_f^3T^3C_F}{5184}\right.\\
&\qquad+n_f^2T^2\left(\left(\frac{1001}{13824}-\frac{\zeta_3}{16}\right)C_F^2+C_A\left(\frac{\zeta_3}{16}+\frac{217}{4608}\right)C_F\right)+n_fT\left(\left(\frac{3\zeta_3}{16}-\frac{275}{1024}\right)C_F^3\right.\\
&\qquad\left.\left.+C_A\left(-\frac{\zeta_3}{64}-\frac{10933}{27648}\right)C_F^2+C_A^2\left(-\frac{11\zeta_3}{64}-\frac{7009}{13824}\right)C_F\right)\right]\frac{1}{\epsilon^2}\\
&\quad+\left[\left(\frac{21\zeta_3}{64}+\frac{1261}{8192}\right)C_F^4+C_A\left(-\frac{79\zeta_3}{256}-\frac{15349}{12288}\right)C_F^3+C_A^2\left(\frac{19\zeta_3}{128}-\frac{55\zeta_5}{128}+\frac{34045}{36864}\right)C_F^2\right.\\
&\qquad+n_f^3T^3\left(\frac{83}{10368}-\frac{\zeta_3}{72}\right)C_F+C_A^3\left(-\frac{709\zeta_3}{4608}+\frac{55\zeta_5}{128}-\frac{70055}{73728}\right)C_F\\
&\qquad+n_f^2T^2\left(\left(\frac{5\zeta_3}{32}-\frac{\pi^4}{960}-\frac{19}{1728}\right)C_F^2+C_A\left(-\frac{5\zeta_3}{32}+\frac{\pi^4}{960}-\frac{671}{41472}\right)C_F\right)\\
&\qquad+\frac{d_{FA}}{N_c}\left(\frac{1}{32}-\frac{15\zeta_3}{64}\right)+n_f\left(\frac{d_{FF}}{N_c}\left(\frac{15\zeta_3}{32}-\frac{1}{16}\right)+T\left(\left(-\frac{69\zeta_3}{128}+\frac{15\zeta_5}{32}+\frac{35}{384}\right)C_F^3\right.\right.\\
&\qquad+C_A\left(-\frac{23\zeta_3}{64}-\frac{5\zeta_5}{64}+\frac{11\pi^4}{3840}+\frac{8819}{27648}\right)C_F^2\\
&\qquad\left.\left.\left.\left.+C_A^2\left(\frac{671\zeta_3}{768}-\frac{25\zeta_5}{64}-\frac{11\pi^4}{3840}+\frac{65459}{165888}\right)C_F\right)\right)\right]\frac{1}{\epsilon}\right\}\left(\frac{\alpha_s}{\pi}\right)^4, \qquad (53)
\end{aligned}
$$

where d_{FF} and d_{FA} are defined in Eq. (44).

References

[1] P. Nason, PoS TOP **2015** (2016) 056 [arXiv:1602.00443 [hep-ph]].

[2] M. Beneke, P. Marquard, P. Nason and M. Steinhauser, arXiv:1605.03609 [hep-ph].

[3] K. G. Chetyrkin, J. H. Kuhn, A. Maier, P. Maierhofer, P. Marquard, M. Steinhauser and C. Sturm, Phys. Rev. D **80** (2009) 074010 doi:10.1103/PhysRevD.80.074010 [arXiv:0907.2110 [hep-ph]].

[4] M. Beneke, Phys. Lett. B **434** (1998) 115 [hep-ph/9804241].

[5] A. H. Hoang, Z. Ligeti and A. V. Manohar, Phys. Rev. D **59** (1999) 074017 [hep-ph/9811239].

[6] A. H. Hoang, Z. Ligeti and A. V. Manohar, Phys. Rev. Lett. **82** (1999) 277 [hep-ph/9809423].

[7] A. H. Hoang and T. Teubner, Phys. Rev. D **60** (1999) 114027 [hep-ph/9904468].

[8] A. Pineda, JHEP **0106** (2001) 022 [hep-ph/0105008].

[9] A. Czarnecki, K. Melnikov and N. Uraltsev, Phys. Rev. Lett. **80** (1998) 3189 [hep-ph/9708372].

[10] [ATLAS and CDF and CMS and D0 Collaborations], arXiv:1403.4427 [hep-ex].

[11] P. Z. Skands and D. Wicke, Eur. Phys. J. C **52** (2007) 133 doi:10.1140/epjc/s10052-007-0352-1 [hep-ph/0703081 [HEP-PH]].

[12] S. Kawabata, Y. Shimizu, Y. Sumino and H. Yokoya, Phys. Lett. B **741** (2015) 232 doi:10.1016/j.physletb.2014.12.044 [arXiv:1405.2395 [hep-ph]].

[13] J. Kieseler, K. Lipka and S. O. Moch, Phys. Rev. Lett. **116** (2016) no.16, 162001 doi:10.1103/PhysRevLett.116.162001 [arXiv:1511.00841 [hep-ph]].

[14] M. Beneke, Y. Kiyo, P. Marquard, A. Penin, J. Piclum and M. Steinhauser, Phys. Rev. Lett. **115** (2015) no.19, 192001 doi:10.1103/PhysRevLett.115.192001 [arXiv:1506.06864 [hep-ph]].

[15] F. Simon, arXiv:1603.04764 [hep-ex].

[16] A. A. Penin and N. Zerf, JHEP **1404** (2014) 120 [arXiv:1401.7035 [hep-ph]].

[17] M. Beneke, A. Maier, J. Piclum and T. Rauh, Nucl. Phys. B **891** (2015) 42 [arXiv:1411.3132 [hep-ph]].

[18] A. A. Penin and M. Steinhauser, Phys. Lett. B **538** (2002) 335 [hep-ph/0204290].

[19] C. Ayala, G. Cvetic and A. Pineda, JHEP **1409** (2014) 045 [arXiv:1407.2128 [hep-ph]].

[20] C. Ayala, G. Cvetic and A. Pineda, arXiv:1606.01741 [hep-ph].

[21] P. A. Baikov, K. G. Chetyrkin and J. H. Khn, JHEP **1410** (2014) 76 doi:10.1007/JHEP10(2014)076 [arXiv:1402.6611 [hep-ph]].

[22] K. G. Chetyrkin, Phys. Lett. B **404** (1997) 161 [hep-ph/9703278].

[23] J. A. M. Vermaseren, S. A. Larin and T. van Ritbergen, Phys. Lett. B **405** (1997) 327 [hep-ph/9703284].

[24] K. G. Chetyrkin, Nucl. Phys. B **710** (2005) 499 [hep-ph/0405193].

[25] R. Tarrach, Nucl. Phys. B **183** (1981) 384.

[26] N. Gray, D. J. Broadhurst, W. Grafe and K. Schilcher, Z. Phys. C **48** (1990) 673.

[27] K. G. Chetyrkin and M. Steinhauser, Phys. Rev. Lett. **83** (1999) 4001 [hep-ph/9907509].

[28] K. G. Chetyrkin and M. Steinhauser, Nucl. Phys. B **573** (2000) 617 [hep-ph/9911434].

[29] K. Melnikov and T. v. Ritbergen, Phys. Lett. B **482** (2000) 99 [hep-ph/9912391].

[30] P. Marquard, L. Mihaila, J. H. Piclum and M. Steinhauser, Nucl. Phys. B **773** (2007) 1 [hep-ph/0702185].

[31] R. Hempfling and B. A. Kniehl, Phys. Rev. D **51** (1995) 1386 [hep-ph/9408313].

[32] F. Jegerlehner and M. Y. Kalmykov, Nucl. Phys. B **676** (2004) 365 [hep-ph/0308216].

[33] M. Faisst, J. H. Kühn and O. Veretin, Phys. Lett. B **589** (2004) 35 [hep-ph/0403026].

[34] S. P. Martin, Phys. Rev. D **72** (2005) 096008 [hep-ph/0509115].

[35] D. Eiras and M. Steinhauser, JHEP **0602** (2006) 010 [hep-ph/0512099].

[36] B. A. Kniehl, A. F. Pikelner and O. L. Veretin, Nucl. Phys. B **896** (2015) 19 doi:10.1016/j.nuclphysb.2015.04.010 [arXiv:1503.02138 [hep-ph]].

[37] S. P. Martin, arXiv:1604.01134 [hep-ph].

[38] P. Marquard, A. V. Smirnov, V. A. Smirnov and M. Steinhauser, Phys. Rev. Lett. **114** (2015) 14, 142002 doi:10.1103/PhysRevLett.114.142002 [arXiv:1502.01030 [hep-ph]].

[39] S. Bekavac, A. Grozin, D. Seidel and M. Steinhauser, JHEP **0710** (2007) 006 [arXiv:0708.1729 [hep-ph]].

[40] K. G. Chetyrkin, J. H. Kühn and M. Steinhauser, Comput. Phys. Commun. **133** (2000) 43 [hep-ph/0004189]; `www.ttp.kit.edu/Progdata/ttp00/ttp00-05/`.

[41] B. Schmidt and M. Steinhauser, Comput. Phys. Commun. **183** (2012) 1845 [arXiv:1201.6149 [hep-ph]]; `www.ttp.kit.edu/Progdata/ttp12/ttp12-002/`.

[42] P. Nogueira, J. Comput. Phys. **105** (1993) 279.

[43] R. Harlander, T. Seidensticker and M. Steinhauser, Phys. Lett. B **426** (1998) 125 [hep-ph/9712228].

[44] T. Seidensticker, hep-ph/9905298.

[45] J. A. M. Vermaseren, math-ph/0010025.

[46] J. Kuipers, T. Ueda, J. A. M. Vermaseren and J. Vollinga, Comput. Phys. Commun. **184** (2013) 1453 doi:10.1016/j.cpc.2012.12.028 [arXiv:1203.6543 [cs.SC]].

[47] T. van Ritbergen, A. N. Schellekens and J. A. M. Vermaseren, Int. J. Mod. Phys. A **14** (1999) 41 doi:10.1142/S0217751X99000038 [hep-ph/9802376].

[48] K. G. Chetyrkin and F. V. Tkachov, Nucl. Phys. B **192** (1981) 159. doi:10.1016/0550-3213(81)90199-1

[49] S. Laporta, Int. J. Mod. Phys. A **15** (2000) 5087 [hep-ph/0102033].

[50] A. V. Smirnov, JHEP **0810** (2008) 107 [arXiv:0807.3243 [hep-ph]].

[51] A. V. Smirnov and V. A. Smirnov, Comput. Phys. Commun. **184** (2013) 2820 [arXiv:1302.5885 [hep-ph]].

[52] A. V. Smirnov, Comput. Phys. Commun. **189** (2015) 182 doi:10.1016/j.cpc.2014.11.024 [arXiv:1408.2372 [hep-ph]].

[53] P. Marquard, D. Seidel, unpublished.

[54] R. N. Lee and A. A. Pomeransky, JHEP **1311** (2013) 165 [arXiv:1308.6676 [hep-ph]].

[55] A. V. Smirnov and M. N. Tentyukov, Comput. Phys. Commun. **180** (2009) 735 [arXiv:0807.4129 [hep-ph]].

[56] A. V. Smirnov, V. A. Smirnov and M. Tentyukov, Comput. Phys. Commun. **182** (2011) 790 [arXiv:0912.0158 [hep-ph]].

[57] A. V. Smirnov, Comput. Phys. Commun. **185** (2014) 2090 [arXiv:1312.3186 [hep-ph]].

[58] T. Hahn, Comput. Phys. Commun. **168** (2005) 78 doi:10.1016/j.cpc.2005.01.010 [hep-ph/0404043].

[59] G. P. Lepage, CLNS-80/447.

[60] A. von Manteuffel, E. Panzer and R. M. Schabinger, JHEP **1502** (2015) 120 doi:10.1007/JHEP02(2015)120 [arXiv:1411.7392 [hep-ph]].

[61] R. N. Lee and V. A. Smirnov, JHEP **1102** (2011) 102 doi:10.1007/JHEP02(2011)102 [arXiv:1010.1334 [hep-ph]].

[62] R. Lee, P. Marquard, A. V. Smirnov, V. A. Smirnov and M. Steinhauser, JHEP **1303** (2013) 162 [arXiv:1301.6481 [hep-ph]].

[63] M. Czakon, Comput. Phys. Commun. **175** (2006) 559 doi:10.1016/j.cpc.2006.07.002 [hep-ph/0511200].

[64] A. V. Smirnov and V. A. Smirnov, Eur. Phys. J. C **62** (2009) 445 doi:10.1140/epjc/s10052-009-1039-6 [arXiv:0901.0386 [hep-ph]].

[65] D. Wellmann, master thesis, KIT, unpublished.

[66] M. Beneke and V. M. Braun, Phys. Lett. B **348** (1995) 513 [hep-ph/9411229].

[67] Y. Schroder and M. Steinhauser, JHEP **0601** (2006) 051 doi:10.1088/1126-6708/2006/01/051 [hep-ph/0512058].

[68] K. G. Chetyrkin, J. H. Kuhn and C. Sturm, Nucl. Phys. B **744** (2006) 121 doi:10.1016/j.nuclphysb.2006.03.020 [hep-ph/0512060].

[69] K. G. Chetyrkin, B. A. Kniehl and M. Steinhauser, Nucl. Phys. B **510** (1998) 61 doi:10.1016/S0550-3213(98)81004-3, 10.1016/S0550-3213(97)00649-4 [hep-ph/9708255].

[70] V. Sadovnichy, A. Tikhonravov, V. Voevodin, and V. Opanasenko, "'Lomonosov': Supercomputing at Moscow State University." In Contemporary High Performance Computing: From Petascale toward Exascale (Chapman & Hall/CRC Computational Science), pp.283-307, Boca Raton, USA, CRC Press, 2013.

[71] A. L. Kataev and V. S. Molokoedov, arXiv:1511.06898 [hep-ph].